Speleogenesis, geometry, and topology of caves: A quantitative study of 3D karst conduits

Johan Jouves[ab] Sophie Viseur[b] Bruno Arfib[b] Cécile Baudement[b] Hubert Camus[a] Pauline Collon[c] Yves Guglielmi[b]

Abstract

Karst systems are hierarchically spatially organized three-dimensional (3D) networks of conduits behaving as drains for groundwater flow. Recently, geostatistical approaches proposed to generate karst networks from data and parameters stemming from analogous observed karst features. Other studies have qualitatively highlighted relationships between speleogenetic processes and cave patterns. However, few studies have been performed to quantitatively define these relationships. This paper reports a quantitative study of cave geometries and topologies that takes the underlying speleogenetic processes into account. In order to study the spatial organization of caves, a 3D numerical database was built from 26 caves, corresponding to 621 km of cumulative cave passages representative of the variety of karst network patterns. The database includes 3D speleological surveys for which the speleogenetic context is known, allowing the polygenic karst networks to be divided into 48 monogenic cave samples and classified into four cave patterns: vadose branchwork (VB), water-table cave (WTC), looping cave (LC), and angular maze (AM). Eight morphometric cave descriptors were calculated, four geometrical parameters (width-height ratio, tortuosity, curvature, and vertical index) and four topological ones (degree of node connectivity, α and γgraph indices, and ramification index) respectively. The results were validated by statistical analyses (Kruskal-Wallis test and PCA). The VB patterns are clearly distinct from AM ones and from a third group including WTC and LC. A quantitative database of cave morphology characteristics is provided, depending on their speleogenetic processes. These characteristics can be used to constrain and/or validate 3D geostatistical simulations. This study shows how important it is to relate the geometry and connectivity of cave networks to recharge and flow processes. Conversely, the approach developed here provides proxies to estimate the evolution of the vadose zone to epiphreatic and phreatic zones in limestonesfrom the quantitative analysis of existing cave patterns.

Graphical abstract

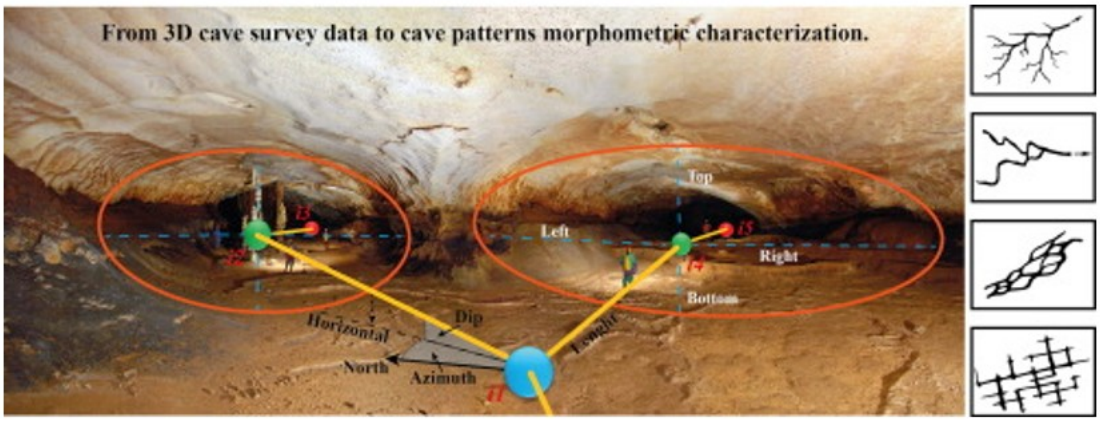

Keywords: Speleogenesis, Karst characterization, Morphometric analysis, Statistics

1. Introduction

The spatial organization of caves has been the focus of many karst research studies for more than a century (Martel, 1921, Renault, 1970, Ford and Williams, 1989, Palmer, 1991, Klimchouk, 2009, Audra and Palmer, 2013). These studies aimed at describing the geomorphological evolution and the position and shape of cave networks according to flow conditions, initial geological discontinuities (e.g., fractures, faults, inception horizons, etc.), and geomorphological landscape evolution. Over the last few years, the karst system behavior has been studied using geostatistical approaches (Renard, 2007, Renard, 2014, Borghi et al., 2016). These approaches reproduce a set of plausible cave networks, termed as simulations, that each fits available static data (e.g., field observations, inlet/outlet points, conduit geometry, partial knowledge of cave networks) and accounts for initial conditions (geological and geomorphological boundary conditions) (Jaquet et al., 2004, Borghi et al., 2012, Borghi et al., 2016, Collon-Drouaillet et al., 2012, Fournillon et al., 2012, Pardo-Igúzquiza et al., 2012, Viseur et al., 2014). A set of simulations can also be used in an inverse modelling process to obtain a spatial distribution of conduits and associated uncertainties (Renard, 2014) by reproducing the hydrograms, thermograms, and chemiograms of springs (Pardo-Igúzquiza et al., 2012, Borghi et al., 2016).

The first step in establishing such stochastic procedures is the quantitative characterization of known three-dimensional (3D) geometries of karst networks in order to consider them as reference field analogues. A few studies focused on 2D/3D cave conduit networks (Howard, 1971, Jeannin, 1996, Frumkin and Fischhendler, 2005, Jeannin et al., 2007, Pardo-Igúzquiza et al., 2011, Albert et al., 2015, Collon et al., 2017) in order to characterize their 2D/3D geometry and connectivity. All these studies considered the surveyed cave network as a whole. However, field geomorphologists identified, by in situ observations, several recurrent cave patterns and proposed to subdivide karst networks into a few types of karst subsystems (Palmer, 1991, Audra and Palmer, 2013, Gabrovšek et al., 2014, Harmand et al., 2017). They showed that independently to initial conditions, karst networks display recurrent cave patterns depending on the involved speleogenetic context, especially the hydrogeological karst zonation, the recharge flow types and the base-level position. For modelling purposes, an interesting question is then to determine whether these cave patterns show significant quantitative differences in their morphometric parameters that can be used in models. Indeed, if these differences exist, the speleogenetic context must be accounted for in modelling workflows, as already performed for initial conditions, which mainly constrain conduit occurrences and orientations.

Thus, we propose to tackle this problem by applying statistical analysis to a wide 3D database of cave conduits that are first decomposed using a manual human expertise. In this paper, the database only includes 3D linear sections corresponding to the recorded passages of the studied cave networks, as it provides a full 3D view of explored cave shapes. The present work is divided into three steps: (i) the building of a database of 3D cave surveys in various speleogenetic contexts (26 caves representing 621 km of conduits), (ii) the splitting of the database according to four main cave patterns, and (iii) the computation and comparison of morphometric parameters using statistical analysis. Notably, the main goals of this study are (i) to test by morphometric analysis on 3D cave networks whether significant differences exist between the recurrent cave patterns and (ii) to provide ranges of morphometric parameters of karst analogues (4 geometrical and 4 topological) to modellers. The paper was also written with a third goal: to show a global methodology to bridge the gap between field karst scientist and modellers.

We had in mind that the readers with field geomorphology or modelling background must understand all the proposed workflow.

We then first describe from a literature review how cave networks can be split into four main types of cave patterns related to four associated speleogenetic contexts and processes. Second, the database and its processing are presented. Third, the eight morphometric parameters selected and the statistical protocol are described. Fourth, the results of the statistical analyses are shown and discussed.

2. Karst systems: an organized aquifer

Karst is defined as a geologic environment containing soluble rocks with a high permeability structure dominated by interconnected conduits dissolved within the host rock. These conduits tend to develop in order to facilitate the fluid flow in the hydraulic gradient direction, wherein the permeability structure evolved as a consequence of carbonate dissolution by circulating fluids (Huntoon, 1995). Limestone aquifer evolution models showed that the positive feedback between dissolution rates and flow rates should result in the formation of caves that are sometimes large enough for people to enter (Ford and Williams, 2007). Karst systems may be addressed in two aspects: their hydrogeological behavior and their geomorphological pattern. From a hydrogeological point of view, the self-organized conduit network, produced by dissolution processes, results in high permeability zones where groundwater flows preferentially, leading to quick responses at springs (Worthington and Ford, 2009). From a geomorphological point of view, the conduit network is self-organized to facilitate an efficient water flow in close relation with landscape evolution and local geology. Cave passages are controlled by passive parameters (lithologic and tectonic) and by boundary conditions (e.g., type of recharge, topographic gradient, base-level position). Previous studies (Palmer, 1991, Häuselmann, 2002, Audra, 2007, Klimchouk, 2009, Audra and Palmer, 2013, Gabrovšek et al., 2014) showed that cave passage profiles and patterns are not randomly distributed but depend on the spatial zonation of karst (i.e., vadose or unsaturated, epiphreatic, and phreatic or unsaturated zones) and on the resulting types of flows.

A geomorphological classification of cave patterns was first proposed by Palmer (1991) who analyzed several thousands of cave passages. In this study, we consider three main cave patterns (Audra and Palmer, 2013) (without the spongework pattern because of the lack of natural analogues in our database), and a fourth one for *water-table* caves (Ford, 1971, Gabrovšek et al., 2014) in order to consider the vertical and horizontal dimension of caves:

• Vadose branchwork (VB): Branchwork cave patterns (planview, Fig. 1) are formed in the vadose zone (cross section view, Fig. 1) by point sources of recharge. The global vadose zone is characterized by water drawn downward by gravity. The downward trend may be interrupted by local ponding where geologic structures cause perched phreatic conditions (Audra and Palmer, 2013). Cave passages exhibit a continuously downward trend along the steepest available openings in the rock. The ideal vadose flow path is straight downward along vertical fractures. Where vertical fractures are not available, canyon passages transmit incoming water. Canyon passages are typically high, narrow, and sinuous. They result in branchwork caves, consisting of stream passages that converge as tributaries. In general, each major water source, such as a doline or ponor, contributes to a single solution conduit, although more than one input can contribute to a single passage. Loops are rare, except where water abandons its original passage for a new one and leads to an older route farther downstream (Audra and Palmer, 2013). At the vadose-phreatic transition, several morphological changes take place in cave passages (Palmer, 1972): (i) the predominant downward trend (canyon and shaft) evolves to tubular and fissure passages; (ii) the overall gradient decreases around 1 $m \cdot km^{-1}$ and the vertical looping segment grows; and (iii) the trend for vadose passages to follow the steepest available path gives way to trends that have no consistent relation to the dip direction of the rock.

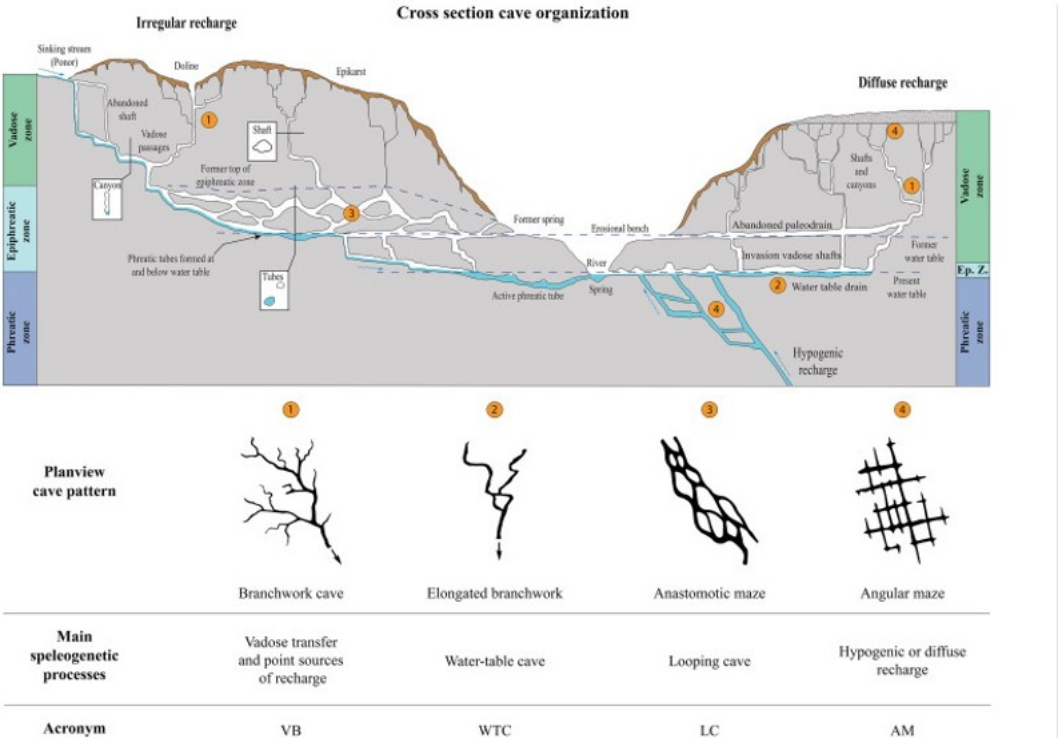

Fig. 1. Idealized cross section of a karst system with a vertical spatial zonation of karst, and planviews of associated patterns. Recharge can be epigenic, with diffuse or concentrated infiltration, or hypogenic. (1) The vadose zone (above the water-table) is characterized by branchwork patterns with tree-like ramifications. Shafts and canyons, with free-surface streams, converge as tributaries. (2) In cases of diffuse recharge and a long-time steady base level, water-table caves are formed at or just below the water table. The groundwater follows a relatively low gradient to springs in nearby valleys. As the flow is still ordered, cave passages exhibit elongated branchwork patterns of tubular phreatic sections comprising few loops. (3) In cases of transient recharge, especially for caves fed by fast runoff and/or sinking streams, the phreatic passages may be unable to transmit all the incoming water; and complex looping overflow routes form in the epiphreatic zone (zone of water-table fluctuation), resulting in looping caves and anastomotic maze patterns. As the base level drops and the surface river entrenches downward, phreatic passages tend to be drained through diversion routes. The former epiphreatic zone is liable to still be active because of the juvenile karst system developed. (4) Angular mazes are formed in prominently fractured rock either by gradual seepage through overlying or underlying insoluble strata, by hypogenic water, or locally by ponded floodwater. Modified after Palmer (1991) and Audra and Palmer (2013).

• Water-table cave (WTC): An elongated branchwork pattern is defined in this study to take the singular character of water-table caves (WTC) into account. When a karst is overlain by a thick semipermeable cover that acts as a filter, the recharge fluctuation is low. The regulated seepage induces a rather steady transfer. Flooding and the development of an epiphreatic zone

are very limited. The main drains concentrate at the water-table level where the water flow is continuous. Cave systems display low-gradient passages with extensive pools. Similar long profiles are characteristic of through-caves fed by extensive impermeable catchment areas. When such caves reach the mature stage, their passage size is large enough to allow the transfer of all stages of flow, including seasonal peaks (Audra and Palmer, 2015). Such through-caves are frequent in monsoonal southeast Asia (Laos, Vietnam, China, Thailand, Philippines) (Audra and Palmer, 2013), in high soluble rock types such as gypsumand rock salt in Iran (Bruthans et al., 2010), or in the northern Apennines (Italy) in Emilia Romagna gypsum areas (Columbu et al., 2015).

• Looping cave (LC): Anastomotic maze patterns are generally formed along bedding planes or fractures by floodwater in the epiphreatic zone. In the most common case, caves always exhibit an epiphreatic zone. In the event of a diffuse and regulated recharge by low transmissive caprock, this zone is limited to a few centimeters to a few meters, leading to water-table caves. When the caves are fed by fast runoff, the transient recharge may allow an even more developed epiphreatic zone, reaching hundreds of meters (e.g., Bärenschacht system in Switzerland, described in Häuselmann et al., 2003). Anastomotic passages are composed of curving tubes that intersect in braided patterns that have many closed loops. The development of looping caves has been recently reinterpreted to be generally epiphreatic and usually forming in the zone of periodic floodwaters and irregular flow rates fed by sinking streams, or by rapid infiltration through a bare karst surface (Audra and Palmer, 2013, Gabrovšek et al., 2014).

• Angular mazes (AM) are formed in a prominently fractured rock. They can be the result of gradual seepage through overlying or underlying insoluble rock, hypogenic water, or ponded floodwater. Network caves are angular (even rectangular) grids of intersecting fracture-controlled fissures. Many are produced either by steady seepage through overlying or underlying insoluble rock or by periodic epiphreatic flooding. Fewer are formed by hypogenic processes, but these include the largest examples such as the Ukrainian caves (Klimchouk, 2009), Brazilian caves (Klimchouk et al., 2016), or sulfuric acid water table caves in France, Austria, and Sicily (De Waele et al., 2016). In this study, the available angular maze network pattern data have been recognized to come from the hypogenic recharge type.

Most of the observable caves appear, however, to have a polygenic history caused by changes in boundary conditions. Thus, different karst patterns can be interconnected in a single cave. In order to study the geometrical organization of caves, we analyzed 3D cave surveys for which the speleogenetic context is known. Each 3D cave survey was separated into elementary cave patterns according to speleogenetic processes that are geomorphologically described.

3. Cave database

In this study, a 3D cave database was built from 3D linear sections provided by caver groups. This data set was mainly acquired in Europe but also in Asia and the USA (Fig. 2). The settings of the studied caves and their associated numerical database are described in the following sections.

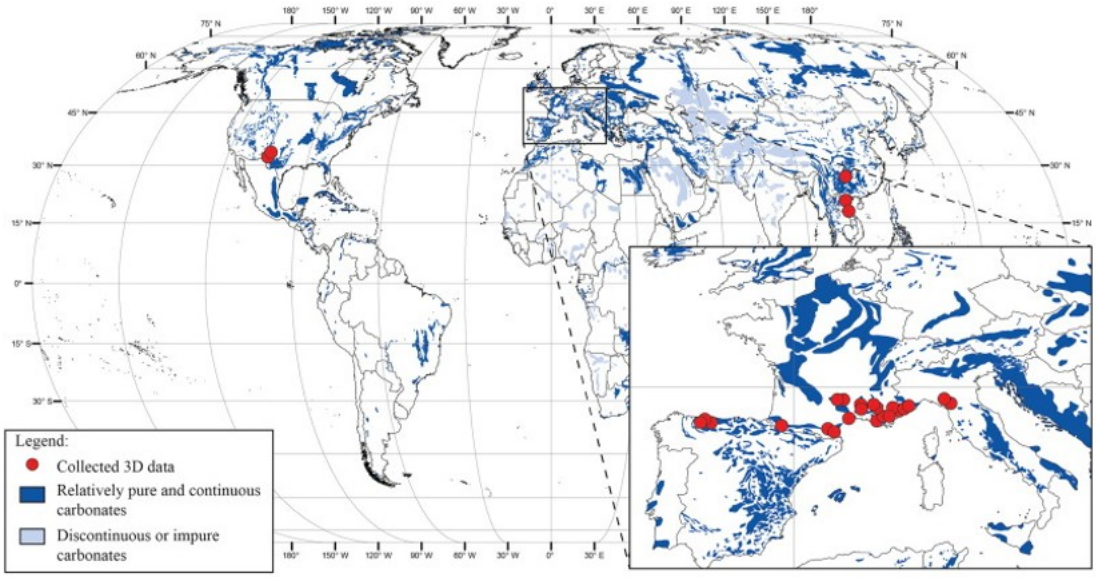

Fig. 2. Location of collected 3D cave survey data plotted on a world map depicting the distribution of carbonate rocks (the principal host rock for karst). Modified from Ford and Williams (2007).

3.1. Cave settings and classification

Among the 50 collected cave networks, only 26 were selected because of their representative data (e.g., length and profile) and known speleogenetic history. These 26 cave networks provided a total of 621 km of karst networks, corresponding to various speleogenetic contexts (Fig. 2 and Appendix A). The database was structured and used as follows:

• Pre-processing of the 3D cave survey to remove field survey bias (see next section); and
• Visualization in 3D of the survey to identify manually the four main geomorphological cave patterns (Fig. 3).

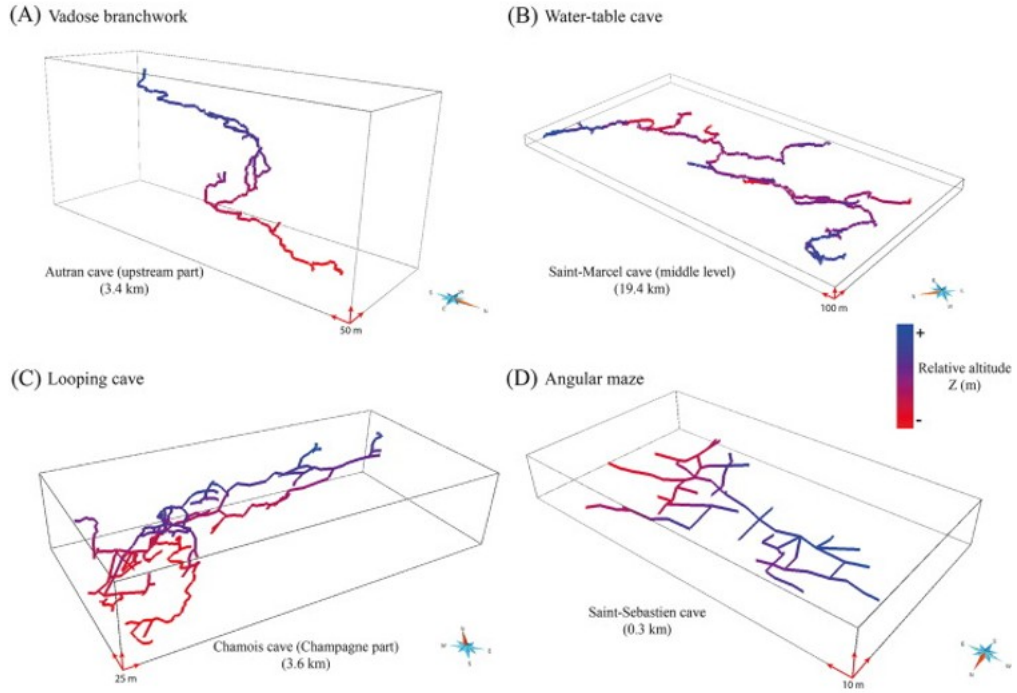

Fig. 3. Examples of 3D cave survey data and their monogenic assignment. The data set was gathered thanks to the invaluable exploration and survey work of cavers. A relative altitude scale is indicated to ease the 3D view.

For polygenic caves, the cave survey was split into the previously defined four groups of cave patterns. Thus, each part of the studied caves was assumed to result from one main speleogenetic process and to represent a virtual monogenic cave pattern sample. Each monogenic cave pattern assignment was validated thanks to the known type of speleogenesis deduced from field observations (direct in situ observation or literature review). As a result, for the whole database all the (virtual or not) monogenic karst samples were assigned to one of the four cave patterns (VB, WTC, LC, and AM) as presented in Fig. 1, Fig. 3. The 26 cave networks include 8 polygenic caves, and the remainder are monogenic. This processing leads to 48 monogenic karst samples (Table 1). It accounts for a total of 73, 749 surveyed stations. The VB type (vadose branchwork) is the most abundant in the monogenic cave pattern sample (37.5%) with 18 samples. The AM type (angular maze) is the least common in terms of number of samples (7

samples) but accounts for the longest surveyed length (> 307 km). In this study, all AM samples are hypogenic. The WTC (water-table cave) and LC (looping cave) types account respectively for 29.2% and 18.8% of the monogenic cave samples.

Table 1. Summary of analyzed cave patterns after monogenic subdivision (VB: vadose branchwork, WTC: water-table cave, LC: looping cave, AM: angular maze) (for more details, see Appendix A).

	VB	WTC	LC	AM
Number of samples	18 (37.5%)	14 (29.2%)	9 (18.8%)	7 (14.5%)
Original monogenic	7	2	3	7
Virtual monogenic (stemming from polygenic)	11	12	6	0
Min. length (m)	177	358	456	189
Max. Length (m)	60,354	53,398	22,950	237,724
Total length (km)	104.0	161.0	48.6	307.4

Virtual monogenic cave samples are the most common type, except for the AM pattern which is only encountered as original monogenic samples. Notably, even if the Carlsbad cavern and Lechuguilla cave contained several monogenic hypogenic patterns (Hill, 1987, Polyak et al., 1998, Palmer and Palmer, 2000, Palmer and Palmer, 2012, Polyak and Provencio, 2001, Kirkland, 2014), individualizing these morphologies was not possible because of the lack of proper information. These two networks were therefore considered as a whole and were assumed to be representative of the AM type.

The database is composed of karst networks stemming from different locations (Fig. 2) and then different surrounding rock types, structural features, climatic settings, etc. The representativeness of this database and its use in this study are explained in Section 4.1.

3.2. The numerical database: preprocessing and assessment

Speleological work provides a 3D description of the basic conduit cave geometry and network (Fig. 3, Fig. 4). However, cavers can only explore a limited part of the conduit networks. They can only map conduits with a minimum diameter of around half a meter accessible by a human being.

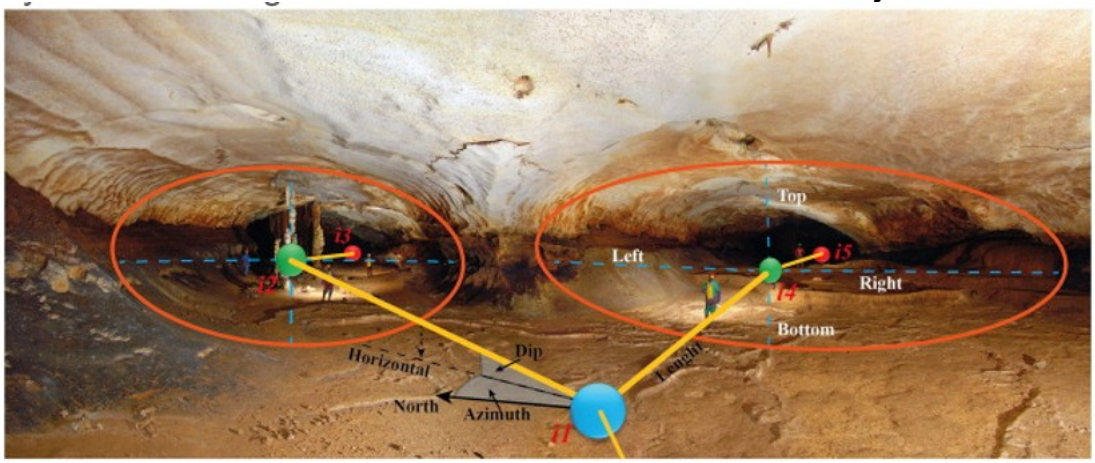

Fig. 4. Example of numerical data in a real cave context. Color circles represent survey stations with node valence ratio (see Fig. 5 for details); the yellow line the survey shot with distance, orientation, and dip; the orange circles the convex approximation of width and height. In numerical data, local properties of width and height are stored on nodes, and fine details are lost. Photo: V. Ferrer. Saint Marcel cave, France.

The original survey data are composed of a baseline and a sequence of survey stations with local width and height (Fig. 4). Between two consecutive topographic stations, the recorded data are the length, the azimuth, and the

dip of the line joining these two stations. From this original information, the absolute or the relative (x_i, y_i, z_i) coordinates of each station S_i can be computed. The original data set was first imported into the speleological software VisualTopo[1] or GHTopo[2], which enables common survey formats to be read and exported in a more standard format (e.g., dxf). These data were then imported into the Gocad 3D geomodeler software[3] as curve objects in order to process and analyze them (Fig. 3).

Cave survey data are originally intended to produce cave maps for cavers and speleological investigations. They may contain ambiguous, approximate or imprecise information that has no impact on map building but that may strongly affect the numerical analysis of the cave network. For this reason, the data set must be cleaned using two preprocessing steps. An automatic preprocessing step is first performed using the Karstmod Gocad plug-in (Collon et al., 2017). During this step, corrections are applied on missing connections (e.g., only a few centimeters separate survey points at cave conduit intersections because of approximations). The second pre-processing step is manual and generally necessary to ensure the representativeness of the network. Indeed, data may contain artifacts such as: *artificial* cycles that correspond to loops acquired in a huge conduit or a room; small cycles owing to survey inaccuracy; fictive data that connect several entrances; and splay shots corresponding to several survey segments that converge at one point in order to describe the local conduit geometry. Thus, these segments do not correspond to cave passage segments but to cave cross section segments. This preprocessing step is handmade and performed in accordance with the knowledge of cave surveying techniques (Jeannin et al., 2007) and cave passages.

Other errors may also exist between the survey sessions owing to the different generations of surveys and the different constraints and habits of cave surveyors. For instance, the quantity and location of surveying stations were determined to suit the convenience of cave surveyors rather than following speleogenetic criteria, such as choosing the two ends of one monogenic segment or imposing a predefined sampling strategy. Thus, despite the preprocessing steps, the database can still contain some errors, though we have attempted to choose and define morphometric parameters that are as insensitive as possible to these errors.

4. Morphometric analysis of cave patterns

4.1. Approach and method

Morphometric approaches to caves were first applied by Howard (1971) on 2D cave systems. Howard (1971) used three topological indices derived from graph theory in order to describe their topological complexity. Later, several authors (Jeannin, 1996, Frumkin and Fischhendler, 2005, Jeannin et al., 2007, Pardo-Igúzquiza et al., 2011, Fournillon et al., 2012, Albert et al., 2015, Collon et al., 2017) defined several indices to describe the complexity of 3D karst features. Statistical approaches were also proposed to highlight the best indices that describe the cave network structures. However, most of these studies consider karst systems as a whole without analyzing a priori genetic and speleogenetic contexts of the cave networks. Consequently, characteristics are averaged over the whole cave network. In this study, the cave surveys were split and clustered according to their speleogenetic context, as previously described in Section 3.1. The objective was to use multivariate statistics on morphometric parameters in order to determine whether significantly different pattern attributes can be related to the speleogenetic contexts.

As mentioned in Section 3.1, the database of karst networks includes several locations and then initial conditions (e.g., rock type, climatic settings). On one hand, several authors (Palmer, 1991, Audra and Palmer, 2013, Gabrovšek et al., 2014) showed that the studied cave patterns are mainly controlled by the speleogenetic context, whatever the other conditions. The other factors would more impact cave conduit occurrence, location and orientations (Palmer, 1991, Filipponi et al., 2009, Filipponi et al., 2010, Tîrlă and Vijulie, 2013, Sauro, 2014, Jacek, 2015, Littva et al., 2015), or local shape variability (Palmer, 1991, Palmer, 2007, Klimchouk and Ford, 2000). On the other hand, this paper aims to test if the targeted morphometric parameters are significantly different from a cave pattern to another one. An underlying issue of knowing the initial conditions (e.g., structural features, climatic settings) is to determine whether factors other than the speleogenetic contexts may interfere on the statistical results. For this purpose, the database should include: (i) all the different cave patterns sharing the same geological and climatic settings, and (ii) a detailed review of these settings for each karst network. However, such a database is hardly

possible, even impossible to obtain. Considering all these points, we opted for the following assumption: as the database includes several setting conditions for each pattern, it corresponds to a representative sampling of the karst network statistical population, stratified according to the speleogenetic context and performed through expertise, i.e., not randomly performed (Cochran, 1977). As a consequence, we first only focused on comparing means and median to limit potential impact of side effects and errors. Only the Kruskal-Wallis testing and box-plot comparisons were then performed. Similarly, only PCA and correlation coefficient analyses were studied as multivariate approaches. Second, the defined parameters must account for three constraints:

• Parameters should be representative of the global network architecture apart from their local conditions (e.g., fractures, faults, bedding planes, inception horizons, changes in boundary conditions, gradient). Thus, the orientations and distribution of karst conduits are not taken into account in this study because they mainly reflect local conditions and not the generic organization of cave conduit networks (Palmer, 1991, Filipponi et al., 2009, Audra and Palmer, 2013, Gabrovšek et al., 2014, Collon et al., 2017).

• Parameters should be as insensitive as possible to cave survey errors.

• Parameters should be mostly invariant to the cave network size.

Thus, towing to the database structure, the factors are not specifically deconvolved; but by choosing parameters that are a priori not impacted by these factors and by comparing the means and median, this study is a first step in trying to determine if quantitative differences exist between these cave patterns. At least, it allows us to show these differences on the basis of a stratified sampling of the cave population. As a consequence, this database can serve as analogue for modelling purposes to integrate adequate morphometric parameter ranges depending on cave patterns.

Finally, for theses analyses, as performed in Fournillon et al. (2012) and Collon et al. (2017), the set of polylines that describes a cave network sample was considered as a set of connected cave *branches* composed of nodes (i.e., survey stations). These authors have defined the branches in different ways. The approach used here is similar to the one proposed by Collon et al. (2017): a cave branch B_j is the j^{th} polyline of a cave conduit between stations corresponding to either an extremity or an

intersection node (Fig. 5). The connected cave branches may form two kinds of *graphs* (Fig. 5): (i) the *complete graph*contains all polyline nodes (intersections, 2-neighbor nodes, and extremities) and (ii) the *reduced graph* is composed only of intersection nodes, external nodes (i.e., extremities), and edges (i.e., the links between these graph nodes). In the following sections, we consider the indices *i* as the i^{th} nodes, *j* as the j^{th} branches.

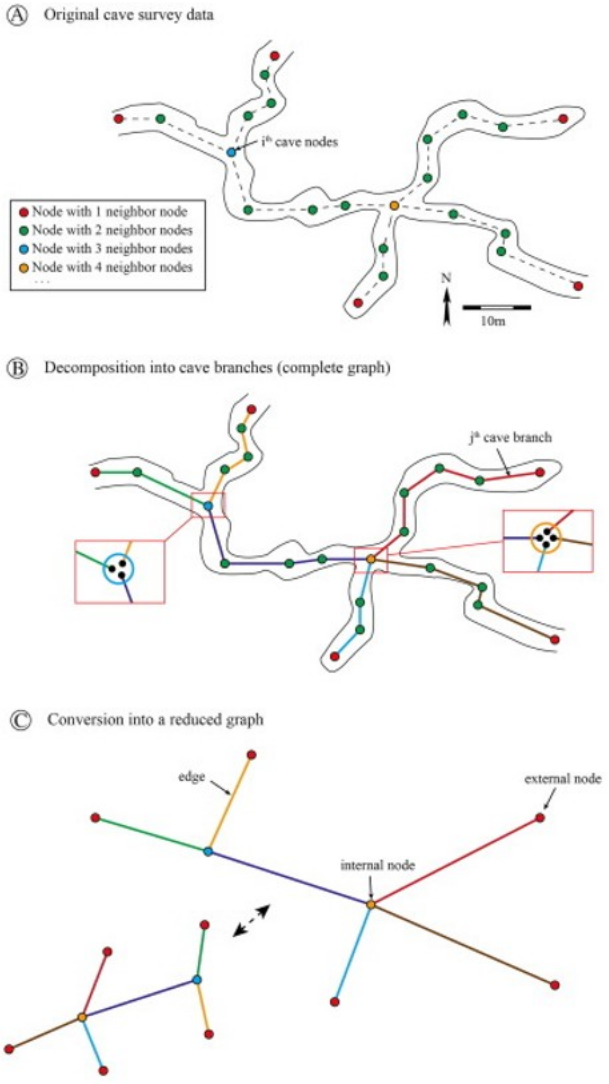

Fig. 5. Principle of the considered data structure from original cave survey data. (A) Scheme of survey data with the defined connectivity degree of node. (B) Cave branch decomposition and resulting complete graph (considering nodes with 2 neighbor nodes). (C) Survey data considered as a mathematical reduced graph: as the geometry (length and orientation) has no obvious meaning in topology, the two graphs are similar (homeotopic).

4.2. Morphometric parameters

4.2.1. Geometrical parameters

Three kinds of geometrical characteristics were computed: the conduit cross section shape (the width-height ratio), the sinuosity (the curvature and the tortuosity), and the vertical vs. cumulative development of the cave passages (vertical index). The width-height ratio and the curvature are computed at each node *i*, the tortuosity on each branch *j*, and the vertical index on each cave sample.
The parameters computed locally (per node or per branch) were averaged over the cave network in order to obtain one value per cave sample. The definition of these parameters is presented below:

Width-height ratio (WH): From the original data, a local width (W_i) and height (H_i) can be obtain to compute the WH-ratio (WH_i) at a node *i* of a cave sample passage:
(1)WHi=WiHi
This ratio gives the relation between horizontal and vertical developments of the conduit cross section at station *i*. The attribute *WH* of a cave sample corresponds to the average value over the cave sample passages, it yields:
(2)WH=1n∑i=1nWHi
where *n* is the number of cave passage nodes.
Ideally, $WH_i = 1$ should correspond to a circular section, $WH_i > 1$ and $WH_i < 1$ are conduit sections more developed along, respectively, the horizontal or the vertical direction (Fig. 6). However, as shown in Fig. 6, the local measured sizes are not necessarily the extremumones, which may lead to bias when computing WH_i. Nevertheless, the attribute used is the average value over the cave passage *WH*. The variability caused by station measurements should then be minimized. Moreover, when one of the local measurements of width or height was not available, like in intersection or for data missing, the WH_i of station *i* was not taken in account.

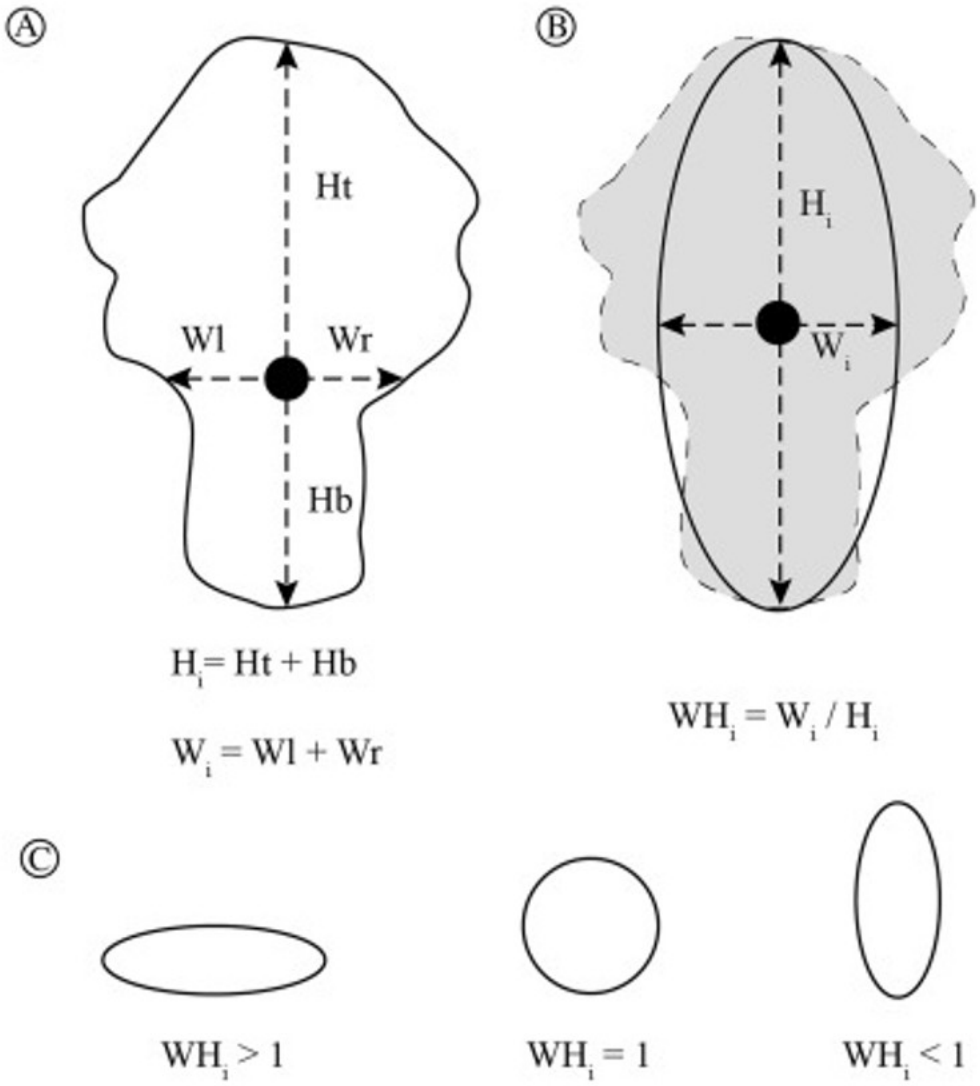

Fig. 6. Processing of width-height ratio for a cave survey station *i*: (A) In-situ measurement of width (W_i) and height (H_i) during the cave survey, at a location chosen by the caver; (B) WH-ratio WH_i calculated from the in-situ measurement for an idealized shape of karst conduit. Fine details are lost; (C) Schematic cave conduit cross sections. Modified from Pardo-Igúzquiza et al. (2011).

Tortuosity (T): Tortuosity was first introduced to characterize river morphology (Brice, 1960, Howard et al., 1970, Hong and Davies, 1979). Tortuosity, also called the sinuosity index, has often been used to describe cave geometry (Jeannin et al., 2007, Pardo-Igúzquiza et al., 2011). Here, tortuosity is computed at the scale of cave branches, i.e., passage parts between ends or junctions (Collon et al., 2017) (Fig. 7). For each branch, the cumulated length of all segments between the two branch extremities (curvilinear length, L_j) and the straight distance between them (Euclidean length, D_j) are calculated (Fig. 7). The ratio between curvilinear and straight

distances, for each branch of a cave sample, gives the tortuosity T_j of the j^{th} branch. Then, the tortuosity T for the cave sample is computed by the average of the T_j values:

(3)Tj=LjDj

(4)T=1nb∑j=1nbTj

where n_b is the number of branches of the cave passage.

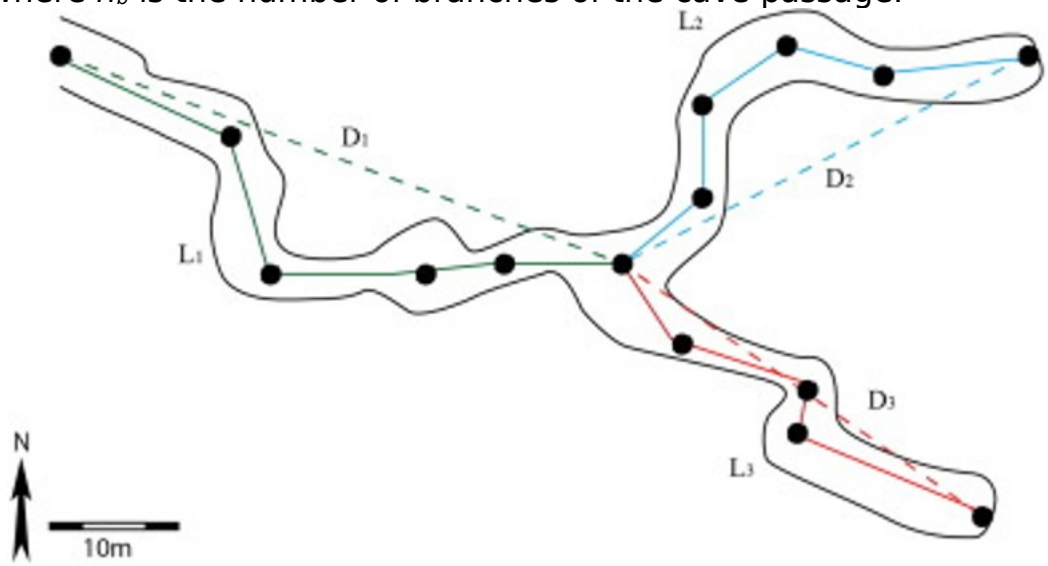

Fig. 7. Sketch of a karst sample divided into three branches. The curvilinear length *Lj* and the Euclidian length *Dj* can be computed along each branch *j*. Then, the tortuosity of each branch is calculated.

Notably, tortuosity depends on the resolution of the cave survey and the ramification of the network. The station locations are generally chosen for the surveyor's convenience, and the tortuosity can be locally either over- or underestimated. However, based on knowledge of surveying techniques (Jeannin et al., 2007) and the authors' survey experience, cave surveys are usually done by minimizing the number of survey stations while obtaining the most faithful representation of the in situ reality. Moreover, similarly to the *WH-ratio*, the tortuosity is averaged over the cave passage, which tends to minimize this arbitrary variability.

The curvature (K): Another way to characterize the sinuosity of the cave passages is the curvature *K*. Considering a curve (*C*) defined by an origin *O* and a curvilinear abscissa *s*(Fig. 8), the curvature at a point *P* of (*C*) is defined as follows:

(5)KP=1r=dtds=d2OPd2s

where *r* is the radius of the osculating circle at *P* (Fig. 8), *s* is the curvilinear abscissa, and *t*is the local tangent vector.

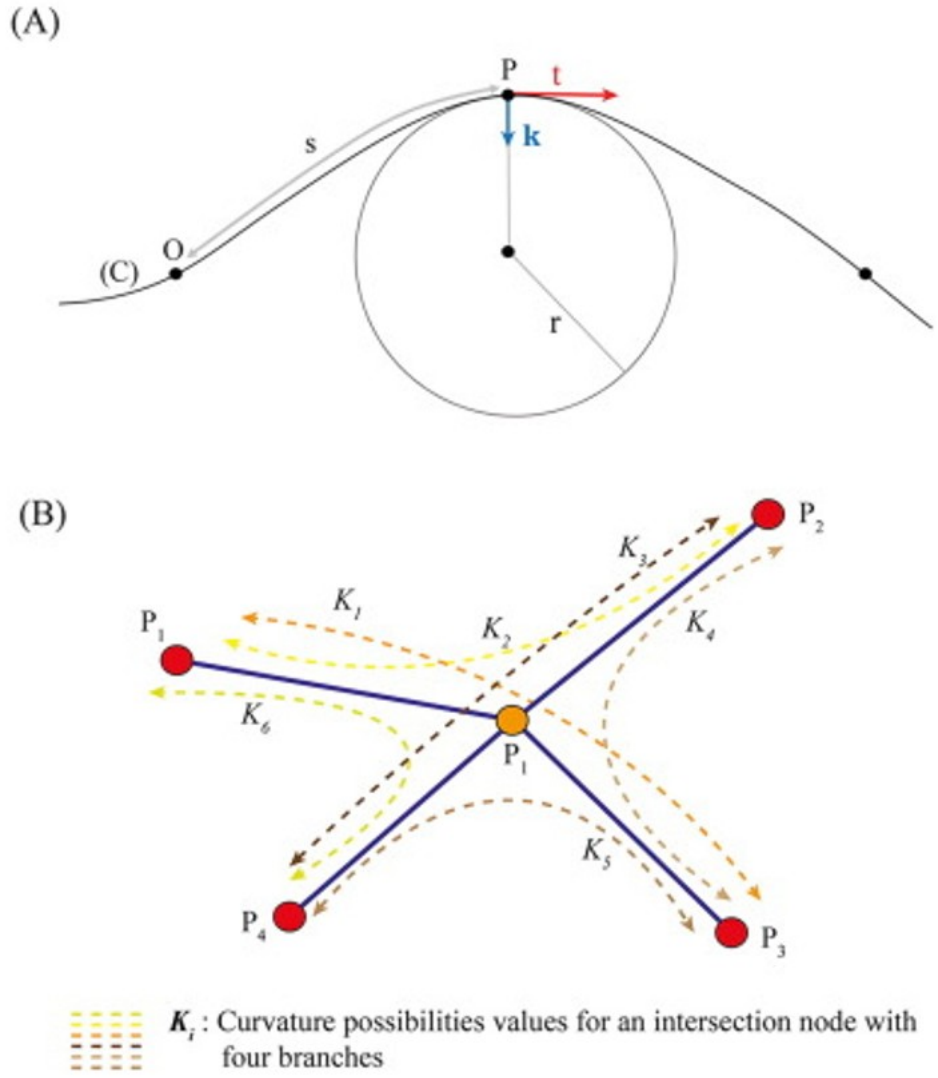

Fig. 8. Curvature parameter computation: (A) Curvature at a point *P* of a curve *C,* where the point *O* is the origin of the curvilinear abscissa *s*. The parameter *k* is the curvature vector and *t* designates the tangent vector at *P*. The value *r* is the radius of the osculating circle at *P*. (B) Possibilities of curvature values computed at an intersection node P_1.

We used the cave survey path as a polygonal line, whose nodes (survey stations) are the points *P*. On a polygonal line, the derivatives are approximated at a point *P* using the 2 neighboring points. However, problems arise at extremities and at intersection nodes. Curvatures at extremities cannot be computed. For intersections, all the combinations of 3-point paths were computed, which involved computing C_2^u (combination number of 2 among *u* points) curvatures for an intersection node with *u* neighboring nodes. This computation was performed using the Gocad-Skua suite and an ad-hoc C ++ code for dealing with intersection points.

High curvatures show high variations in conduit directions, which can differentiate straight cave passages from angular ones. To obtain this kind of information from a cave sample passage, the curvature attribute *K* used in this paper corresponds to the mean of the absolute values of curvature K_i along this passage:

(6)K=1n′∑i=1n′Ki

where *n'* is the number of 3-point combinations along the passage. Curvature parameter differs from tortuosity because it is computed at nodes and because it is influenced by locally high values corresponding to dramatic changes in directions. Two curves may have the same tortuosity and different curvature parameter values and vice-versa (Fig. 9).

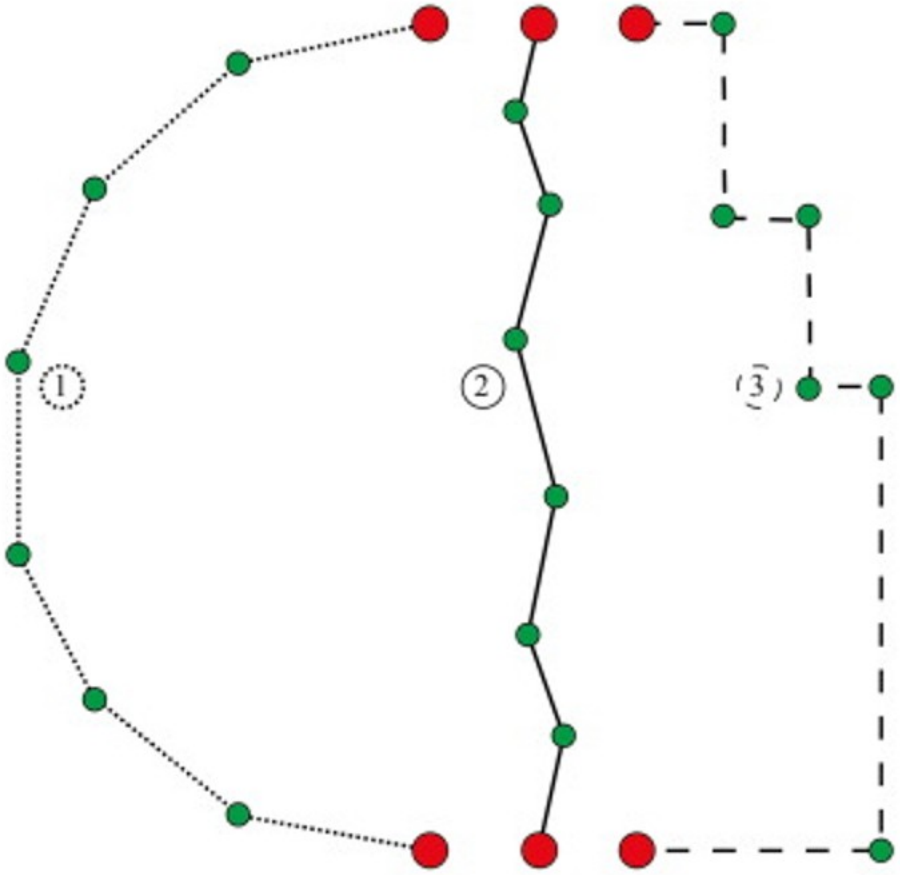

Fig. 9. Example of three curves with similar tortuosity *T* or curvature *K*. Curves (1) and (2) have a similar curvature while the curvature is higher in (3). Curves (1) and (3) have a similar tortuosity while (2) is lower.

The vertical index (V): The vertical index *V* was introduced by Piccini (2011) to describe the vertical vs. horizontal development of a cave network. It is defined as the ratio between the vertical developments of a cave conduit network (i.e., total depth *Td*) on its 3D total length development (Fig. 10):

(7)V=Td∑j=1nbLj

where L_j is the length of the *j*th cave branch of the cave sample, and n_b is the number of branches.

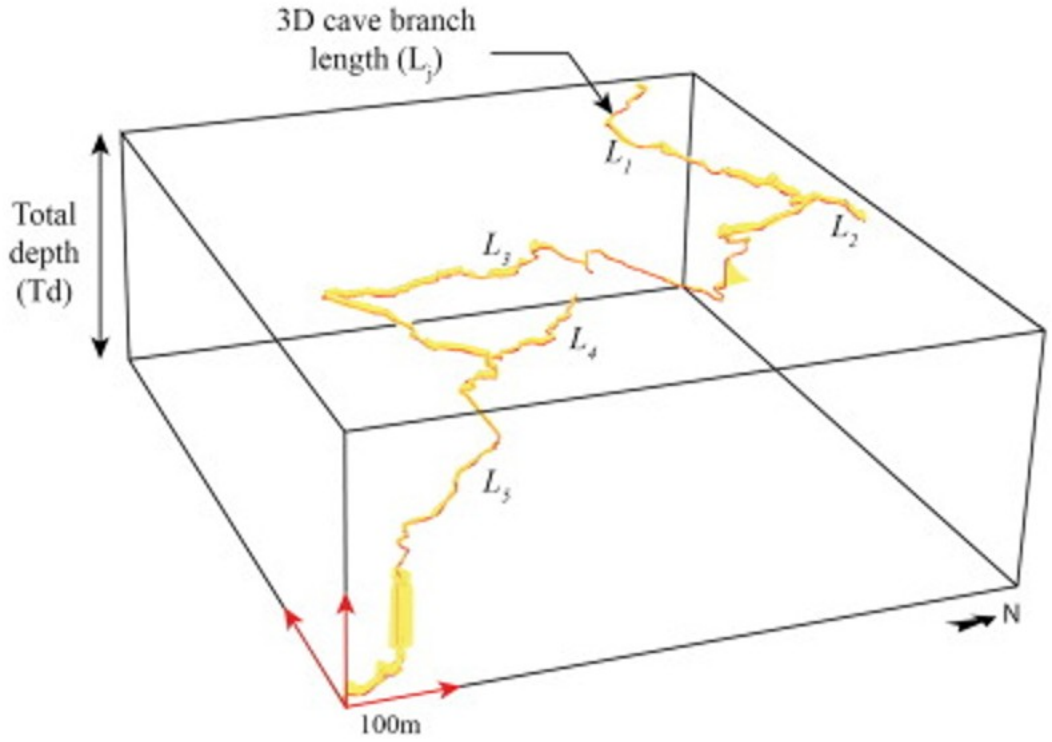

Fig. 10. Computation of the vertical index *V* on a 3D cave sample: the total depth *Td* is represented as the height of the bounding box and the total length L as the cumulative curvilinear length of the cave passage. The red line corresponds to the surveyed passage, and the yellow surface to the triangulated surface of the surveyed conduits.

V theoretically ranges from 0 to 1. Cave samples with *V* close to 0 are those more fully developed in the horizontal plane or with many branches around the same elevation level. High values of *V* indicate preferentially vertical elongated organizations. For instance, perfectly vertical pits with a small plan length have $V \approx 1$. Many small vertical caves in the infiltration zone of alpine karst have $V > 0.8–0.9$ (Piccini, 2011).

4.2.2. Topological parameters

As presented in Section 4.1, from a mathematical point of view the network of conduits may be seen as a graph in which the stations are graph nodes connected by a collection of edges (Fig. 5). The graph used here only accounts for nodes that are leaves (ends) or junctions, termed a *reduced graph* (Fig. 5). The number of nodes is termed N ($N \leq n$) and the number of edges E. Four topological parameters were used to characterize the network structure and connectivity: (i) the node connectivity degree, (ii) alpha and (iii) gamma graph indices, and (iv) the ramification index (R).

Node connectivity degree (Nd_u): The node connectivity degree (Nd), also called node valence, corresponds to the number of neighbor nodes connected by an edge to this node (Fig. 5). The Nd_u refers to the total percentage of nodes with u neighbors over a karst sample considered as a graph: Nd_1 for end-lines, Nd_3 for an intersection at three edges, etc.

Graph indices (γ and α): Different indices have been defined since the 1960s by scientists working in quantitative geography (Haggett and Chorley, 1969, Rodrigue et al., 2006). These indices were used to characterize the topology of transportation networks (Garrison, 1960, Taaffe and Gauthier, 1973) and were also applied on cave systems (Howard, 1971) in order to quantify the cave network connectivity. In this paper, we use the two most important indices termed the α and the γ indices (Barthélemy, 2011).

In a general definition, the γ index is defined by

(8)γ=EEmax

where E is the number of edges and E_{max} the maximum possible number of edges if all the N nodes are connected to each other (i.e., in the case of a complete graph). The γ index is a measure of the network density and $\gamma \in]0:1]$.

Similarly, the α index (or “meshedness”) is expressed by:

(9)α=ΓΓmax

where Γ is the number of elementary cycles (i.e., the cyclomatic number equal to $\Gamma = E - N + 1$) and Γ_{max} the maximum possible number of elementary cycles for a complete graph. An elementary cycle is a path loop that does not contain other subloops. This index ranges over [0; 1] and is equal to 0 for a linear or a tree graph.

Two graph cases may be encountered: planar and nonplanar graphs. A planar graph is defined as a graph that can be embedded in a plane in such a way that its edges intersect only at their endpoints. The two indices are defined for planar and nonplanar cases as a function of *E* and *N* (Barthélemy, 2011) as follows:

	Planar	Nonplanar
α	α=E−N+12N−5	α=2E−N+1N−1N−2
γ [a]	γ=E3N−2	γ=2ENN−1

a. For graphs composed of two nodes and an edge, γ is assigned to the value 1.

Howard (1971) proposed to consider cave networks as planar graphs as they are only locally nonplanar. Indeed, using different equations will make comparison difficult between cave networks. On the one hand, the use of the planar formula for locally nonplanar cases overestimates the values of both indices. On the other hand, it will discriminate much better between locally nonplanar cave networks that are in some respects more complicated than planar ones. We therefore decided to use only the formula for planar cases.

The ramification index (R): This parameter is introduced in this study and aims at discriminating braided from tree-like networks. It is defined by

(10)R=∑u=3umaxNduNd1

where u_{max} is the maximum node valence of the graph.

R index represents the ratio between junctions and extremities. High values represent networks with many ramifications with respect to extremities. Thus, *R* discriminates networks with meshed-like structures. Values close to 0 represent linear or tree-like graphs.

To summarize, high values of *α*, *γ*, and *R* should show roughly more complicated graphs with more intersections, loops, and edges.

4.3. Statistical protocol

Once morphometric parameters have been computed on each cave sample, statistical analyses were performed using the XLSTAT[4] add-on for Excel. All the statistics (e.g., means, variances, etc.) were computed on the same database. The statistical procedures aimed at (i) highlighting whether speleogenetic processes lead to significant differences in the mean of a

given morphological parameter and (ii) determining the relationships between variables.

To test whether significant differences exist between means of a morphometric parameter, the nonparametric Kruskal-Wallis (KW) hypothesis test was used, which accounts for the number of samples per class and the parameter variability. The risk α was set arbitrarily to 0.05 in this study, as commonly performed in geoscience applications. This test aims at determining whether significant differences exist between means of the morphometric parameters according to family type. The null hypothesis H_0 considers that the means of a morphometric parameter are similar for every speleogenetic type (as there are 4 groups: $m_1 = m_2 = m_3 = m_4$, where m_k is the mean of the morphometric parameter of the k^{th}speleogenetic type). The alternative hypothesis H_1 considers that at least one mean differs from another one (e.g., $\exists\ k\ ,\ l \in [1; 4]\ ,\ m_k \neq m_l$). In this study, a risk $\alpha = 5\%$ is chosen, which means that if the computed p-value is $< 5\%$, the H_0 hypothesis is rejected. In that case, it means that at least one mean of a group is different from the others. We then used the post-hoc test of Steel-Dwass-Critchlow-Fligner for multiple comparison procedures (Hollander et al., 2013) with the Bonferroni correction to show which groups are significantly different and which are similar. Notably, multiple comparison testing is less robust than the Kruskal-Wallis test and may lead to inconsistent results. In these cases, the p-value is generally close to 5% and must be reinterpreted to show the binary results. To discuss the KW results, we will also use boxplot diagrams to show the maximum, minimum, median, lower, and upper quartiles.

The second purpose was to determine whether any correlations between variables exist and whether these relationships differ between the different speleogenetic contexts. First, correlation coefficients were studied as well as their significance. Second, the parameters that showed significant differences from the KW test were selected for Principal Component Analysis (PCA), one of the most frequently used multivariate data analysis methods (Saporta, 2006). It projects observations from a p-dimensional space with p variables to a lower k-dimensional space ($k < p$) with k principal components while preserving the maximum amount of dispersion (i.e., variance) from the initial dimensions. If the information associated with the first two or three axes represents a sufficient percentage of the total

variability of the scatter plot (usually 80%), the observations can be represented on a 2D or 3D plot respectively, thus making interpretation much easier. Moreover, PCA allows the structural correlation of variables to be highlighted. Correlation circles and contribution calculations allow us to determine the correlations between variables and principal components.

5. Results

5.1. Quantitative analysis of cave patterns

5.1.1. Morphometric comparison

The Kruskal-Wallis (KW) test revealed significant differences on all the computed parameters as a function of cave patterns. A summary of the KW test for the parameters analyzed and each cave pattern is given in Table 2.
Table 2. Summary of the Kruskal-Wallis test for the analyzed parameters and each cave pattern; colors refer to groups discriminated by the Kruskal-Wallis test with a risk α = 5%: light color corresponds to low values, dark color to high values; the values given are the mean and standard deviation of the analyzed parameters.
Considering the geometrical parameters only, we see that

- By considering the vertical index V, the tortuosity T, and the WH-ratio parameters, the vadose branchwork type (VB) is distinguished from the water-table cave (WTC), the looping-cave (LC), and the angular maze (AM), which are considered as equivalent. Thus, without considering the curvature K, VB ≠ WTC = LC = AM.
- The behavior of K is different. The KW test highlights that WTC < VB = LC < AM, i.e., the curvature distinguishes WTC and AM (which are geometrically different) from VB and LC (which are considered equivalent).

Using the topological parameters, the differences are more complex. The first main result is that WTC ≈ LC concerning the topology of the reduced graphs. For VB and AM, their connection to this WTC-LC group depends on the parameter:

- When R and α are considered, VB < WTC ≈ LC ≈ AM. This is then similar to the main geometrical trend.
- When γ is considered, VB ≈ AM > WTC ≈ LC.

To summarize, considering all the parameters (except for the curvature), it seems that WTC ≈ LC, as expected from karstological studies. They seem to be the most similar cave patterns in this study. The WTC and LC types are topologically quite similar, with relatively high ramified structures containing few loops (low α index). Conduits are more developed in the horizontal plane (low value of V) and are more circular and/or horizontally elongated (high value of WH). Notably, VB is the most different pattern from a geometrical point of view. The VB type is steep ($V = 0.327$), more sinuous ($T = 1.38$), with mean variations in conduit directions and with vertically elongated conduit sections ($WH = 0.616$). The VB pattern has the weakest connected and ramified structure ($R = 0.574$) with few loops ($\alpha = 0.012$). However, the graph density is high ($\gamma = 0.501$) owing to the presence of very simple reduced graphs (with 2 or 3 nodes only) leading to a high density value γ. The AM type differs significantly from the other patterns, exhibiting the highest quantity of loops ($\alpha = 0.065$) and angular ramified passages ($K = 0.324$). High values of R and γ indicate strongly ramified and connected structures. However, only hypogenic AM were available in the studied database.

The KW test thus reveals differences between cave patterns. To support this analysis, the distribution of the parameters was scrutinized through boxplots (Fig. 11). Globally, the results of the boxplots are in agreement with the results of the KW test. Figure 11and Table 2 show that in the VB type, the values of V, T, and γ are highly dispersed and have a higher median value than the other monogenic types. Considering the same parameters, the other types WTC, LC, and AM are not differentiated and have range values that are not very variable (minimum and maximum: $0.005 \leq V \leq 0.17$; $1.05 \leq T \leq 1.44$; $0.33 \leq \gamma \leq 0.41$). The distribution of the curvature values (Fig. 11C) of the WTC and AM types are highly different with median values of $K_{med\ WTC} = 0.106$ and $K_{med\ AM} = 0.326$, respectively. Concerning the WH ratio, Fig. 11D shows that the VB type differs markedly from the other groups with a median value of 0.56, whereas the median is > 1.63 for the other three types. An equivalent distribution of the parameter R is observed in Fig. 11E, with an increasing value for pattern types VB < WTC < LC < AM. For α, AM has by far the highest median. A decreasing trend is observed for T from VB to AM. The parameter γ seems more

stationary considering the median, even if similarly to the KW test, WTC and LC show slightly lower median values.

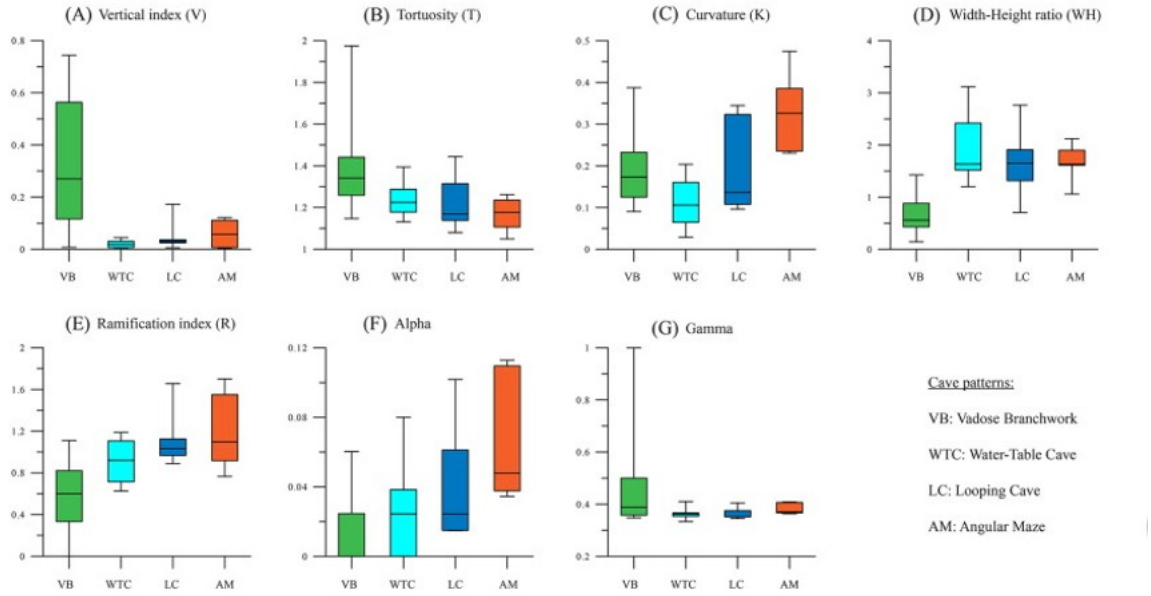

Fig. 11. Boxplots showing the distribution of the computed parameters for each monogenic type. (A) Vertical index, (B) tortuosity, (C) curvature, (D) WH ratio, (E) ramification index, (F) α graph index, and (G) γ graph index. The caps at the end of each box indicate the extreme values (minimum and maximum), the box is defined by the lower (p25) and upper (p75) quartiles, and the line in the center of the box is the median.

According to the KW test and boxplots, three groups may be differentiated. First, the VB type has the most vertically elongated structures and conduit cross sections and the most tortuous conduits with small variations in conduit directions. Considering R and α (without γbecause of the very simple reduced graph cases with high values), the VB type has the least ramified organization. Second, the WTC and LC types are topologically and geometrically close to each other, as pointed out by the KW test and as can be seen in Fig. 11. The LC type has higher extreme values (third quartile and maximum) of K, R, and α parameters, meaning potentially more angular, ramified, and looping passages; while conduit cross sections of the WTC type are preferentially horizontally elongated. Focusing on the Rparameters (i.e., the ratio between junction and termination nodes), WTC, LC, and AM seem to be equivalent. Thus, regarding the total number of nodes of the reduced graph, they have the same number of junctions, except that the number of α cycles is higher for the AM types. Thirdly, the AM type appears to have

the most complex organization, with a meshed ramified structure and with the highest number of loops and angular intersecting conduits.

5.1.2. Geometrical cave pattern correlation

The 2D cross plots (Fig. 12) show correlations between the four geometrical parameters (*V*, *T*, *K*, and *WH*). The Fig. 12A (*V* vs. *WH*) clearly shows two groups of dots: the VB pattern with *WH* essentially < 1 and *V* between 0 and 0.8, and the other three patterns with *WH* > 1 and *V* < 0.2. The couple *WH*/*V* reflects, for VB, a morphology of conduits that are preferentially vertically elongated (*WH* < 1) with a variable verticality. In the vadose zone, we find the signatures of in situ observations (Fig. 1): the shafts (*V* close to 1) and the canyon passages with variable verticality. The less inclined conduits correspond to networks with a preferentially horizontal development, such as groundwater-free surface rivers, or the meander type.

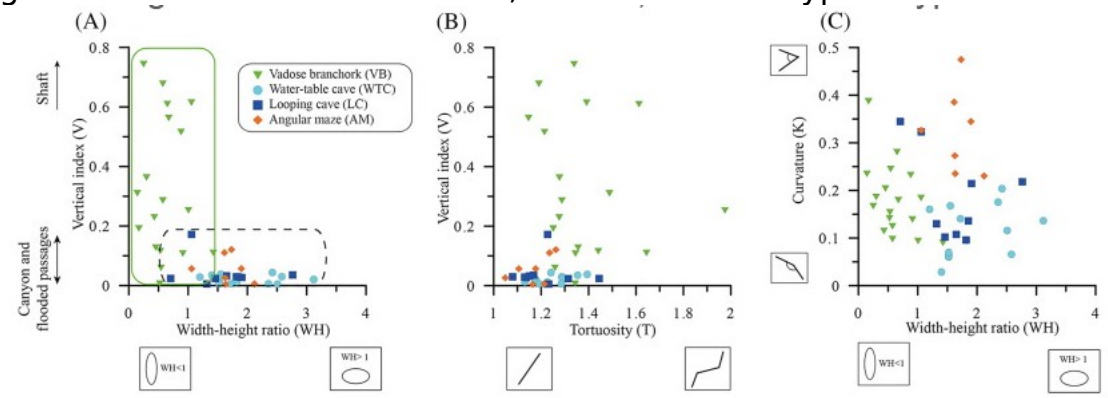

Fig. 12. Cross-plot showing the distribution of geometrical parameters (*V*, *WH*, *T* and *K*) for the 48 monogenic cave samples. Values for the polygenic network (i.e., before monogenic subdivision) are not plotted and are shown in the following section.

The Fig. 12B (*V* vs. *T*) shows that tortuosity is variable for all the cave patterns and is not linked to the verticality of cave branches (*V*).

On Fig. 12C, it may be observed that VB, WTC, and AM are mostly in separate areas:

- The VB type is mainly delimited by *WH* < 1, with high variability for *K*.
- The WTC type is roughly located where *WH* > 1 and K < 0.2.
- The AM type is mostly confined to where *WH* > 1 and K > 0.2.
- The LC type is spread between these zones.

Thus, whatever the verticality of VB, its *WH* ratio is still < 1.5, whereas for the three remaining types, the verticality index is always below 0.2 in the studied database, although *WH* presents a high variability > 0.5. Tortuosity

of the VB conduits does not seem to be linked to the verticality of its branches. Finally, slight correlations may be found between *K*and *WH* for VB and AM. Disregarding AM types because of the specific limitations of the database used in the present study (i.e., the hypogenic origins of all the cave samples), cave samples tend to decrease from VB types with high values of *K* and low values of *WH* to WTC types with fewer changes in orientation directions (low value of *K*) and more elongated conduit cross sections (high value of *WH*). Only the linear correlation coefficients between *WH* and *K* are significant at the 10% level for VB and AM, with respectively -0.45 and -0.66, which corresponds to a weak to medium inverse linear correlation.

5.1.3. Topological cave pattern correlation

In this section, the correlations between the topological parameters (*node valence* Nd_u, R, α, and γ) are studied. As previously mentioned, Nd_2 are not considered.

Table 3 shows the proportion of nodes for a given node valence Nd_u according to each monogenic type, indicating whether the cave samples are linear (only Nd_1), ramified in 3 branches like a tree-graph (occurrence of Nd_3), or in 4 or more branches (occurrence of $Nd_{>3}$, Fig. 4). The values are given in Appendix B. The VB cave samples are mainly made up of Nd_1 nodes (mean of 67.2%) even if the standard deviation is high (17%). The WTC, LC, and AM are quite similar regarding Nd_1 and Nd_3. However $Nd_{>3}$ is noticeably higher for the AM types. In general, the proportion of Nd_1 tends to decrease from VB to AM types to give way to a greater proportion of Nd_3 (or more) in types WTC, LC, and AM. This means that the networks tend to be more lattice-like than tree-like from VB to AM.

Table 3. Proportion and standard deviation of a given node valence Nd_u for each monogenic type.

	Nd_1 (%)	Nd_3 (%)	$Nd_{>3}$ (%)
Vadose branchwork (VB)	67.2 ± 17.0	30.5 ± 15.4	2.3 ± 3.3
Water-table cave (WTC)	52.9 ± 5.6	43.4 ± 6.6	3.7 ± 2.8
Looping cave (LC)	47.7 ± 5.2	46.8 ± 5.4	5.5 ± 2.6
Angular maze (AM)	47.2 ± 7.2	40.8 ± 9.4	12.0 ± 5.7

The Fig. 13A shows the correlation between R and α for the 48 monogenic samples. As previously explained in Section 4.1, the karst network is studied as a reduced graph, and an increase in R shows an increase in the number of extremities with respect to the number of internal nodes in the graph. The low α values are characteristic of linear or tree graphs, and an increase in α reflects an increase in the number of cycles. The α values range from 0 to 0.13. In Fig. 13A, samples for which α is mainly close to 0, R values do not exceed 0.8. For $\alpha \neq 0$, R and α increase according to a general trend. No particular distribution of the four cave patterns is observed along the linear trend.

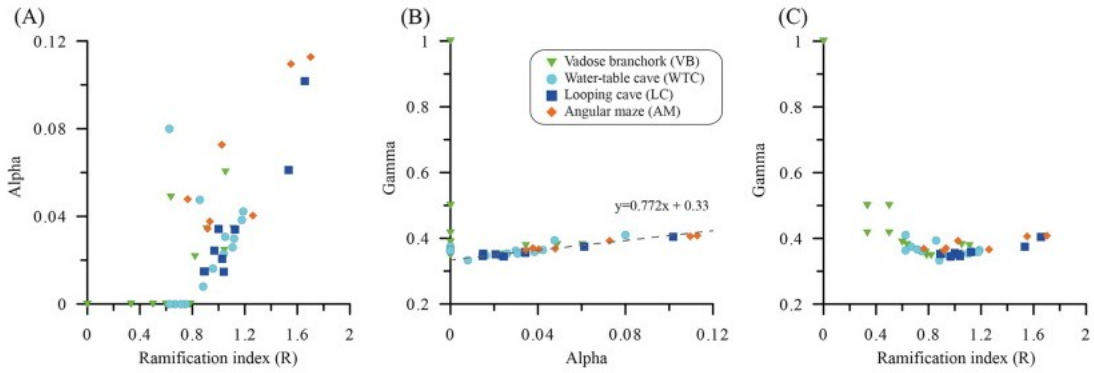

Fig. 13. Cross-plots showing the distribution of topological parameters (ramification index R, α, and γ) for the 48 monogenic cave samples. (A) α vs. R; (B) γ vs. α (the equation is given for the linear trend processed with $\alpha > 0$); (C) γ vs. R. Values for polygenic networks (i.e., before monogenic subdivision) are not plotted and are shown in the following section.

The Fig. 13B shows the correlation between α and γ. The γ index represents the graph density, i.e., the maximum number of edges that can be contained in a graph as a function of the number of nodes. Two zones can be observed in Fig. 13B:

• For $\alpha = 0$, γ ranges from 0.36 to 1. It includes only VB and WTC cave samples. This is mainly caused by the presence of very simple graphs composed of 2 or 3 nodes only, in which the combination of edges is very low, hence a high value of the density γ. As Nd_2 nodes were not taken into account, some cave passages were converted into very simple graphs, such as: a linear path with n nodes into a graph with 2 nodes and an edge and a Y path into a graph composed of 3 nodes.

• For $\alpha > 0$, the samples are distributed along a linear increasing trend between α and γ. Correlation coefficients, as well as their significance presented in Table 4, confirm a strong global linear relationship as they do

not consider samples with $\alpha = 0$. In the case of VB and WTC, the relationship is not significant or weak respectively. A simple regression performed on samples for which $\alpha \neq 0$, on 32 monogenic cave samples, shows that the linear trend between α and γ can be expressed as: $\gamma = 0.772\alpha + 0.33$, which reflects the structural correlation expected between α and γ for very large N(see Appendix C): $\gamma=23\alpha+13$.

Table 4. Linear correlation coefficients between topological parameters (R, α, and γ) for each monogenic type and the whole data set (i.e., global); the number of graph nodes is also presented; significant correlation coefficients are denoted in bold.

	VB	WTC	LC	AM	Global
Number of nodes: min/max	2/870	10/410	34/364	29/12,884	59/876
R/α corr. coeff.	**0.65*****	0.24 (no sign.)	**0.94*****	**0.84****	**0.73*****
α/γ corr. coeff.	− 0.37 (no sign.)	**0.60***	**0.97*****	**0.98*****	**0.93***** ($\alpha \neq 0$) (− 0.23 for all values)
R/γ corr. coeff.	**− 0.84*****	− 0.47 (no sign.)	0.91***	**0.80***	**− 0.65*****

* $p < 5\%$, ** $p < 2\%$, *** $p < 1\%$.

The Fig. 13C shows the correlation between R and γ, which is not linear but has a particular shape. This may suggest that a structural relationship exists between R and γ. For this reason, with a confidence index of 95%, a nonlinear regression gives a logarithmic relation between R and γ:

$$(11)\gamma=1+1.21\ln 1+1.21*R2-0.52*R-1.05*R$$

However, this relationship did not help us find an obvious analytical origin because the analytical formulation of R (as a function of E and N) depends on the type of network pattern (e.g., binary tree, n-ary tree, lattice, etc.).

The key point in Table 4 is that depending on the speleogenetic type, the correlations between the topological indices vary in strength and sign. This means that these relationships are not analytically obvious and depend on the network structure, in this particular case, of karst networks. The AM and LC, having more lattice-like networks, seem to have the highest correlations between the topological indices. These first results suggest that further work is required to understand the origin of these relationships in the particular case of cave network patterns.

5.2. Multivariate analysis

The PCA was computed on 45 (virtual and original) monogenetic samples belonging to the four groups. The samples for which $\gamma = 1$ (Fig. 14) were removed because these samples (i.e., 3 samples of the VB type) are outliers with respect to γ, and performing a PCA on the whole database would lead to an overcontribution of these particular samples in defining the F1 axis, which is not desirable for a PCA (Saporta, 2006). The seven input variables (see Table 2) have a mean contribution of 14.28%. The Kaiser criterion (selecting axes for which a contribution is greater than the mean one) led to only two axes being selected. However, in order to reach ~ 80% of the total variance – as usually recommended (Saporta, 2006) – three axes were taken into consideration as axes F1-F2 represent 62.56% and the third axis represents 13.60% of the total variance, which is only slightly below the mean contribution. The total variance expressed by F1-F2-F3 then reaches 76.16%. The third axis F3 is discussed below but is not analyzed through factorial planes as it does not allow individual distributions to be clearly distinguished.

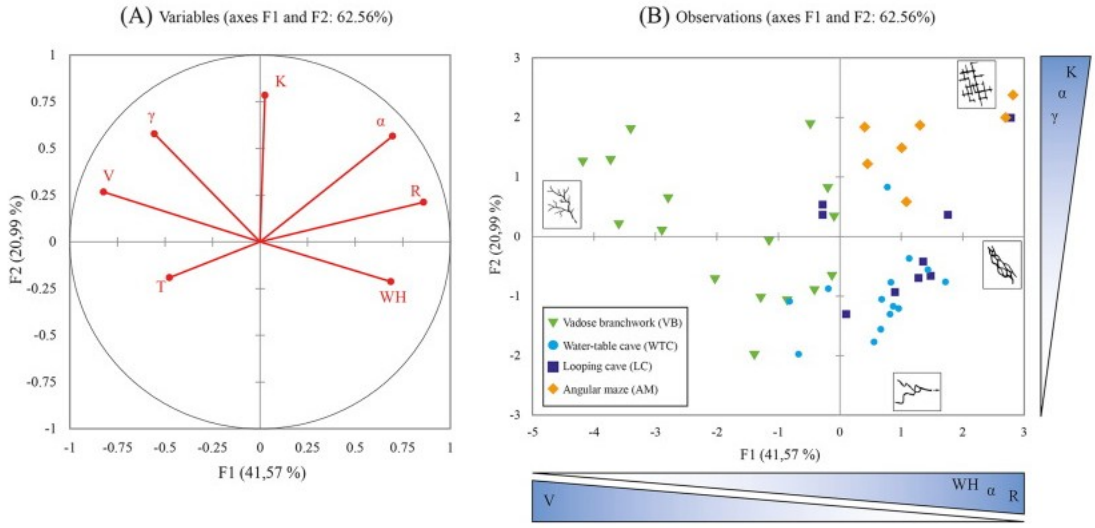

Fig. 14. PCA F1-F2 axis of the 45 monogenic karst samples based on the seven parameters analyzed (without the node valence Nd). (A) Plot of the variables used. (B) Bi-plot of the distribution of monogenic karst samples. The F3 axis representing 13.47% of the total variance is not shown here. The origin of the axes represents the center of gravity of the scatter plot.

Considering the correlation circle (Fig. 14A) and the contributions of the input variables, the F1 axis (first principal component) is supported negatively by *V* and positively by *R*, with respective contributions of 23.3% and 25.4%. The *WH* and *α* also positively contribute to the F1 axis with respectively 16.2% and 16.7%. The F2 axis is mainly positively supported by the curvature *K* with a contribution of 41.9%. The *α* and *γ* parameters also support the F2 axis with respectively 21.8% and 22.7%. The other parameters are not significant enough to be discussed here.

The Fig. 14B shows the distribution of the samples in the factorial plane F1-F2, in which the axis origin corresponds to the gravity center (mean) of the variables. The plot can be divided in three areas:

• The VB type is distributed to the left of the F2 axis (i.e., negative values of F1). The VB type is highly influenced by a strong linearity and verticality, with poorly ramified structures, and thus a potentially dense network (high values of *γ*). However, the distribution is scattered between negative and positive values along the F2 axis, because of high variations of *K*.

• The WTC samples are roughly located in the bottom right of the scatterplot, which corresponds to medium to low curvatures, more lattice-like networks (i.e., high *R* and *α*) containing some loops and more horizontal development (i.e., low *V*).

• The AM samples are roughly located in the right top corner of the scatterplot, which corresponds to high curvature values, highly lattice-like networks (e.g., higher α, R) and horizontal development (i.e., low V). Moreover, as α contributes positively to F1 and to F2, it means that samples located in the top right corner are particularly characterized by networks having a high number of loops.
The LC type is located between the other groups, but it seems to overlap the WTC zone more and the VB zone less. The LC horizontal development and network organization may then be considered as similar to those of WTC and AM, except that the curvature is more variable.

The factorial planes F1-F3 or F2-F3 do not highlight interesting distributions about the different cave patterns. The F3 axis is highly supported by tortuosity (61.5%), which means that tortuosity is independent of the parameters that support F1-F2.

5.3. Polygenic karst networks

Eight polygenic karst networks are available in the database. They were included in the previous analyses as 29 virtual monogenic networks (11 VB patterns, 12 WTC, and 6 LC; Table 1). The Fig. 15 shows the distribution of the polygenic networks (i.e., before monogenic subdivision) with their associated virtual monogenic networks. The distribution of the monogenic samples is addressed in Fig. 12, Fig. 13. The Figs. 15A and B show the correlations between geometrical parameters and Figs. 15C and D, the topological correlations.

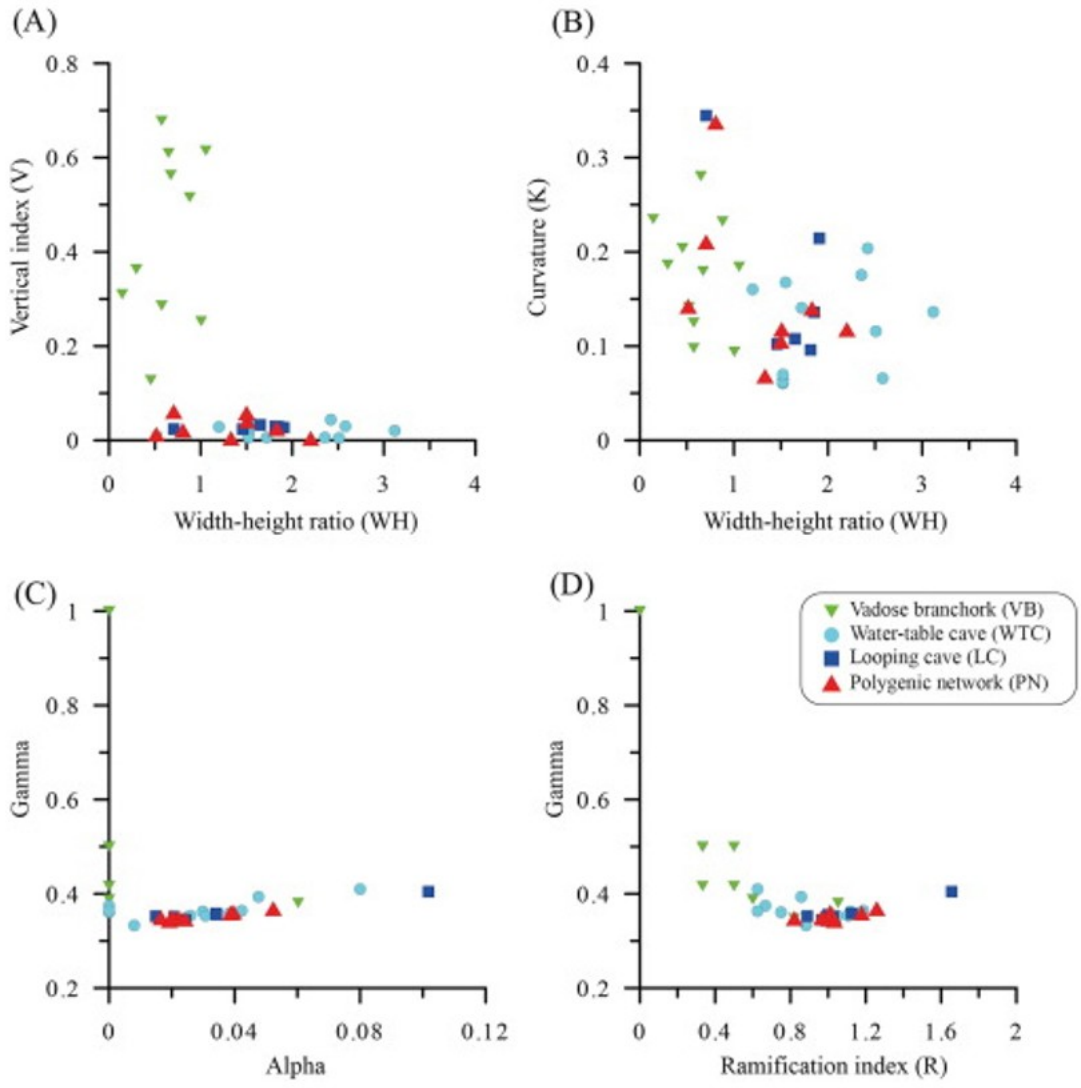

Fig. 15. Cross-plots showing the distribution of geometrical and topological parameters for the polygenic networks (8 samples) and for the monogenic ones stemming from polygenic networks (29 samples). (A) and (B): Geometrical correlations, (C) and (D): topological correlations.

The distribution of parameters is not discussed here in detail, but some general features are given. By analyzing the polygenic networks, the vertical component of the networks (Fig. 15A) is reduced and does not exceed $V = 0.1$. The *WH* ratio remains variable with a smaller range than when considering only the monogenic ones. Only the curvature remains within a range of equivalent variability. From a topological point of view, the variability is much lower and does not provide the resolution obtained with the monogenic networks. The topological indices R, α, and γ are less variable

with values between: $0.821 \leq R \leq 1.259$, $0.017 \leq \alpha \leq 0.052$, and $0.334 \leq \gamma \leq 0.369$.

Table 5 gives the means and standard deviations of the computed parameters for the eight polygenic networks before monogenic subdivision. For all the morphometric parameters studied (geometrical and topological), the polygenic networks are located close to the mean of all the epigenic monogenic networks (VB, WTC, LC).

Table 5. Mean and standard deviation of analyzed parameters for the eight polygenic networks before monogenic subdivision.

Parameters	Geometry					Topology	
	Vertical index (V)	Tortuosity (T)	Curvature (K)	Width-height ratio (WH)	Ramification index (R)	α	γ
Polygenic network	0.029 ± 0.021	1.259 ± 0.092	0.155 ± 0.078	1.30 ± 0.546	1.037 ± 0.124	0.029 ± 0.010	0.354 ± 0.010

Overall, the values in Table 5 and Fig. 15 are less scattered. The comparison with Table 2 is difficult to perform because only polygenic samples are considered here and because, obviously, the final parameter value of a polygenic network is influenced by its predominant speleogenetic type.

6. Discussion and conclusion

The approach developed for the morphometric analysis of four common cave patterns was based on the coupling of geomorphological knowledge and statistical procedures. Eight morphometric parameters were proposed to characterize the karst pattern geometry and topology. These parameters were computed on a database of 48 monogenic cave samples coming from various parts of the world and resulting from different geological, geomorphological, and speleogenetic contexts. The statistical analyses show different behaviors depending on the speleogenetic context. In the following, we summarize and discuss these results and cover also some general questions about the future of cave system characterization and modelling.

6.1. The four cave patterns

To account for differences in speleogenetic contexts, future geoscientists (e.g., modellers, hydrogeologists, reservoir geologists) will have to evaluate the speleogenetic history of the studied karst system in order to assign cave pattern regions. The key points for the determination of the four cave patterns are summarized below:

- Vadose branchwork patterns (VB) are characterized by open-channel flow, in shafts and canyons, converging as tributaries (i.e., tree-like ramifications) and are strongly influenced by geological structure.
- In cases of diffuse recharge and a long-time stable base level, water-table caves (WTC) are formed at or just below the water table and mainly develop along inception horizons.
- In cases of transient recharge, the phreatic passages may be unable to transmit all the incoming water. Complex looping overflow routes form in the epiphreatic zone (zone of water-table fluctuation), resulting in anastomotic maze patterns with many curving tubes (Looping cave, LC).
- Angular maze (AM) patterns are formed in prominently fractured rocks either by gradual seepage, by hypogenic water, or locally by ponded

floodwater, resulting in maze networks of a large percentage of enlarged initial discontinuities.
However, these common cave patterns may be encountered in the same cavity. In this study, we assume that the individualization of cave patterns was done as accurately as possible. Whenever possible, field investigations were conducted. When this was not possible, we based our separations on the literature and on our expertise in 3D cave survey. With this approach, we consider that the monogenic parts thus obtained are representative of the four main cave patterns described. While some errors in the monogenic separation cannot be ruled out, we believe that these errors, if they occur, are only local and have little influence on the results presented. Precise field studies in each cavity would, perhaps, refine this division and the parameter range values.

Another bias to control could be derived from local conditions of cave development, as e.g., geological constraint. In our opinion, comparing karst networks of different origins made it possible to be roughly abstract from local conditions and to highlight cave patterns as a global descriptor. However, another possible way could be to work on a homogeneous cave data set like in a particular region, or in homogeneous geological setting, or in similar climatic contexts. But, such studies are still challenging, as such a homogeneous data set are scarce. Moreover, other cave patterns, such as spongework caves (Palmer, 1991, Audra and Palmer, 2013), usually formed in rocks with high intergranular porosity by the mixing of different water sources with varying degrees of aggressiveness, were not included in this study because of the lack of natural analogues in the studied database. Also, several monogenic hypogenic patterns can be encountered in Lechuguilla and Carlsbad caves. For these two samples, only the global network architecture was analyzed and the different monogenic hypogenic features were not individualized because of the lack of proper information. Morphometric analysis of these special kinds of speleogenesis, i.e., spongework patterns or different kinds of hypogenic features, could provide additional valuable information about the cave network organization.

6.2. Quantifying spatial organization of karst

As a cave survey is originally dedicated to produce cave maps, it could contain some errors for morphometric statistical analysis. Even if numerical tools and handmade procedures were used to reduce these errors, the presented data set could still contain some. It mainly concerns the location of the survey station inside the conduits and the sampling strategy (e.g., sampling step). The representativeness of the used database may also be questioned, even if it corresponds to the foremost published database of karst networks. Nevertheless, the results presented in this study can be interpreted as an encouraging point and help geoscientists to quantitatively characterize the four main cave patterns satisfactorily.

From the statistical analysis (Table 2 and Fig. 14), significant differences exist in the geometry and the topology of the cave networks depending on the speleogenetic context. The schemes proposed by Palmer (1991) (Fig. 1) suggested at first glance that in terms of topology, VB and WTC were opposite to LC and AM, and that in terms of geometry, the sinuosity of WTC and LC looked similar. Thus, our quantitative study shows that the topology and geometry of caves, inferred from the database, do not reflect exactly what was expected. As can be seen in Table 2 and in Fig. 14, two patterns can be easily distinguished: the vadose branchwork (VB) and the angular maze (AM) type. However, the difference is more difficult to highlight between water-table cave (WTC) and looping cave (LC). One of the strengths of this quantitative analysis is that it uses 3D data and so is not influenced by the strong simplifications of a 2D perception. Thus, the differences between real cave morphologies may indeed be more tenuous or gradual. Furthermore, the similarities/dissimilarities exhibited by the analysis can be compared to the qualitative results of previous studies based on field observations (Ford, 1971, Palmer, 1975, Palmer, 1991, Palmer, 2007, Klimchouk, 2009, Audra and Palmer, 2013, Klimchouk et al., 2016). Considering epigenic cave networks only (i.e., VB, WTC, and LC), the geometrical and topological parameters analyzed are in agreement with in situ observations made by karst scientists. In the vadose zone, VB patterns are characterized by a strongly linear and sinuous organization with vertically elongated conduits. At the bottom of the unsaturated zone, the WTC and LC patterns are closely related and differences depend only on the recharge variation conditions. Thus, morphological differences are tenuous,

as both patterns are characterized by a low vertical index V, a high width-height ratio WH (Fig. 12A), relatively low sinuosity, but more curvilinear and more ramified cave conduits (Figs. 12B, C and 13). For WTC and LC, the couple $\{V < 0.2$ and $WH > 1\}$ reflects flooded flows (dissolution occurs on all the walls) with a verticality of cave networks close to the slope of the piezometric surface (water table). However, some differences can be distinguished in the geometrical and topological organization. Indeed, the water-table cave type (WTC) is strongly characterized by smooth curving tubes (Fig. 12C), with a planar structure, meaning a development along horizontal planes (e.g., inception horizons) close to the water table. In Fig. 12C, the Looping cave type (LC) is spread between the VB (vadose branchwork) and WTC types. This distribution is consistent with in situ observations. Indeed, LC karst conduits are usually observed in situ (Fig. 1) at the interface between the vadose zone and the saturated zone (or paleosaturated zone). The LC type is thus subject to water table fluctuations that generate the development of alternative flow paths in the epiphreatic zone and thus an increase in topological indices such as α and R. The Fig. 14 demonstrates the general geometrical and topological trends that characterize a karstic pattern. Overall, it opposes the VB type to the others. This may be explained by the type of flow responsible for the dissolution of karst conduits. While the vadose zone is characterized by branchwork patterns with open-channel flows converging as tributaries, the other types are formed under phreatic or epiphreatic flows, resulting in an increase in dissolved initial discontinuities and thus in topological complexity. The source of recharge may also differentiate the distribution of samples. The AM type has the highest topological complexity. This can be explained by the type of fluid responsible for the establishment of karst drains. In this study, AM maze patterns result from the host-rock dissolution by hypogenic fluids assumed to have a higher aggressiveness, which involves a high degree of enlarged discontinuities. Thus, the type of flow and the source of aggressive water strongly control most of the morphometric differences in cave pattern topologies and morphologies.

Finally, the correlation of quantitative indices with speleogenetic processes shows the importance of considering the type of genesis in terms of geometry, architecture, and connectivity to obtain a karst conduit system characterization. Over the last decade, new exploration and survey tools

have emerged. They simplify the acquisition process and allow finer resolutions of 3D data. LiDAR or photogrammetry technology are now used in underground survey, making it possible to analyze 3D morphologies of small portions of conduits and drains (Jaillet et al., 2011, Ployon et al., 2011, Sadier, 2014). The morphometric analysis of such data will provide valuable information on micro- and meso-scale karst conduit geometries.

6.3. About the morphometric parameters

The parameters analyzed can also be scrutinized. The results show that the VB patterns can be characterized by high tortuosity and variable curvature values, whereas AM caves display the opposite behavior with low tortuosity and high curvature values. From a geometrical point of view, VB caves are characterized by few ramified networks and may be sinuous. Then, as the tortuosity is computed per cave branch, this explains the possibility to have high values in the case of VB networks. On the contrary, AM networks are highly ramified. Thus, even if changes of direction may be high at intersection points, tortuosity of the branches remains low. These analyses can be correlated to speleogenetic processes. In the case of LC and AM patterns, the cave structures use all potentially draining discontinuities (leading to more changes of direction) even if they are not on the regional flow-path direction. In the case of VB samples, networks are conditioned by a gravity flow and are therefore highly selective with respect to the discontinuities used (Jacek, 2015, Littva et al., 2015). Moreover, karst conduits preferentially develop where discontinuity intersections occur because of the mixing of different water- CO_2 compositions (Littva et al., 2015). Thus, variability of the VB cave tortuosity may be linked to the presence of fractures: if fractures exist, they change the local direction of the conduits, and then the more this occurs, the higher the tortuosity is. We should also mention that from a practical point of view, the VB caves are narrow and do not allow us to perform long survey distances between stations: this leads to small local offsets and not large changes of direction (Fig. 16), hence lower curvatures.

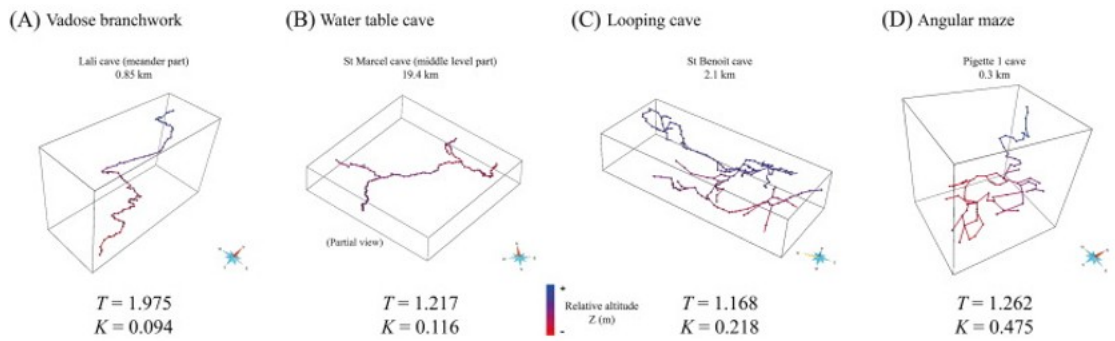

Fig. 16. Examples of real 3D monogenic cave samples with related values of tortuosity *T* and curvature *K*.

A branch-length weighted average of tortuosity would also be interesting to compute in order to account for a more representative tortuosity of the karst network. However, the impact of the length used for weighting branch tortuosity (Euclidian or curvilinear length) must be evaluated. Indeed, Euclidian length may privilege straight branches, and on the contrary, the curvilinear one may favor the highly tortuous branches.

Concerning the use of the α and γ parameters, Howard (1971) suggested that caves with few loops and tree-like patterns, such as VB and WTC caves in this study, should have $\alpha$and γ indices close to 0 and 1/3 respectively (Table 2, Fig. 11, Fig. 13). For more interconnected networks, such as AM and LC ones, these values should be close to 1/4 and 1/2 respectively. In this study, on 3D surveys of natural cave analogues, the density γ is always around or slightly higher than 1/3 (except for very simple reduced graphs with only 2 nodes). The parameter α is mostly very close to zero (mainly < 0.05), and even for the Lechuguilla cave, which is very complex, it is only 0.11. Howard (1971) worked on 2D projected maps, which may explain these differences. The values of this study are in agreement with those obtained recently by Collon et al. (2017). Some values differ slightly in the present study because of the data cleaning (Section 3). However, considering the genetic type, a deeper analysis is performed giving smaller range values for each parameter and monogenic type. In this study only α, γ and R, were analyzed. For further studies, other topological parameters could also be tested, such as those recently proposed by Collon et al. (2017). As they suggested, the average vertex degree of the reduced graph of networks (k) characterizes the interconnectivity of the systems and correctly

discriminates strongly interconnected systems (mazes) from acyclic ones (tree-like structures).

6.4. From morphometric parameters to models

A lack of knowledge concerning the internal system of a karst aquifer can limit the accuracy of karst network models as well as the effectiveness of pipe-flow models (Peterson and Wicks, 2006, Hartmann et al., 2014). Indeed, the routing of flow through a karst system is intrinsically linked to the geometry and the topology of the system. The correlation between speleogenetic processes and quantitative parameters provides a way to condition and/or validate such models.

First, the database of real karst network analogues built here provides a thorough database enriched by speleogenetic information and cleaned, as far as possible, of survey errors. Second, this study shows the importance of considering the type of genesis for quantitative karst reservoir characterization. Range values of parameters according to speleogenetic processes are proposed for eight morphometric parameters. The *WH* and its variability along the passage (WH_i) can be used to simulate the shape of conduits in an ODSim approach (Henrion, 2011, Rongier et al., 2014) according to the speleogenetic type and thus to provide accurate simulations of 3D karst conduit morphologies. The distribution of *WH* can also be useful to condition the flow and hydrodynamic behavior of karst conduits in an inverse modelling procedure (Borghi et al., 2016).

Even if it has been studied, tortuosity is difficult to account for in a modelling approach and is not robust enough to characterize sinuosity. However, in the cases of preferentially vadose branchwork developed karst systems, tortuosity can be used by hydrogeologists to estimate the real length of tracer tests: $L = L_e$ x T (with L the real length of path along a flow line, $L_e$the Euclidian length between the injection point and the restitution point, and T the tortuosity index) (Goldscheider et al., 2008). As it can be seen in the analysis, the real flow distance should not be higher than two times the linear distance. However, even if we have not computed these parameters, we think that in cases of more lattice-like systems, such as WTC, LC, and AM ones, the total sinuosity index (P_T) (Hong and Davies, 1979, Mosley, 1981, Egozi and Ashmore, 2008) could be a more relevant indicator of the possible real flow path.

Another need in geostatistical simulation methods is the relative proportion of karst conduits with respect to the *matrix* (not considered as a conduit at the modelling scale). Some authors (Worthington, 1999, Bonacci et al., 2006, Klimchouk, 2007) reported that the average effective porosity value of a karst massif generally varies from 0.1 to 1%. However, to account for speleogenetic contexts, the proportion of each karst type is also required. This means that further studies are necessary to define these relative proportions. As an example, Albert et al. (2015) provided an estimation of the macroporosity for hypogenic systems, reporting values between 1 and 2%.

A further legitimate question is to determine whether the nonhumanly accessible parts are similar to the accessible ones. Some authors (Jeannin et al., 2007, Pardo-Igúzquiza et al., 2011) proposed that caves have typical fractal dimensions close to 1.67. However, the organized structure of a karst system and the morphometric differences stemming from the speleogenetic contexts make a unique fractal dimension questionable. As an example, Hendrick and Renard (2016) reported self-similar structures with a fractal dimension around 1.5 for maze coastal karst networks of Tulum (Quitana Roo, Mexico). Thus, we may consider that karst networks are not characterized by a single fractal dimension but potentially several, depending on the type of speleogenesis, and hence cave patterns.

To conclude, stochastic simulation procedures of cave networks (Jaquet et al., 2004, Henrion, 2011, Borghi et al., 2012, Borghi et al., 2016, Collon-Drouaillet et al., 2012, Fournillon et al., 2012, Pardo-Igúzquiza et al., 2012, Viseur et al., 2014) require quantitative input parameters that characterize natural analogues. In this study, morphometric parameters were computed on each cave sample from different geological and karstological contexts. Thus, this database is representative of a wide range of karst analogues and can be used in two different ways: as input parameters for modelling approaches or as validation data. The average values are given in Appendix B. Thus, by knowing the evolution stages of a given karstic system, the user can choose the corresponding speleological context and assign the corresponding values. Some parameters are more difficult to directly integrate into a modelling approach as the currently proposed modelling methods cannot take them into account. In this case, the

values can be used in a comparison/validation procedure by calculating these parameters on the simulated networks.

Acknowledgements

The authors would like to thank ParadigmGeo and the AGSA for their support in providing Gocad software and plugins and the RING team of the GeoRessources laboratory for the KarstMod plugin. This research would not have been possible without the invaluable work of generations of cavers in all the caves investigated. We express our thanks to cavers and colleagues who have provided us with 3D karst data and all the cavers who took part in the exploration and topographic survey, with special thanks to: P. Audra, J.Y. Bigot, J. Botazzi, D. Cailhol, J.P. Cassou, S. Clement, M. Faverjon, S. Jaillet, H. Lankester, G. Maistre, and Carlsbad Cavern National Park. This work benefited from fruitful discussions within the framework of the KARST observatory network (www.sokarst.org) initiative from the INSU/CNRS, which aims to strengthen knowledge sharing and promote cross-disciplinary research on karst systems. This work is part of the DARDENNES project funded by the Agence de l'Eau (RMC), the city of Toulon, Veolia Eau, Cenote Company, and Aix-Marseille University. The authors are also grateful to R. Marston, co-editor of Geomorphology, J. De Waele and other anonymous reviewers for their constructive remarks, which helped to improve this manuscript.

Appendix A. Summary of cave surveys used in this study and their speleogenetic separation. Some cave networks are monogenic

Cave	Monogenic subdivision	Length (m)	Speleogenetic dominant process / Hydrodynamic zonation	Host rock formation	References
Abisso Chimera (Apuan Alps, Italy)		9616.2	VB	/	/
Arrestelia (France, Pyrenees)	Arrestelia_VadoseH	60,354	VB	Upper cretaceous	/
	Arrestelia_VadoseV	841.7	VB		
Autran (Aven) (France, Vaucluse)	Autran_Epiphreatic1	593.4	WTC	Barremian and Aptian (Urgonian limestone)	/
	Autran_Epiphreatic2	402.9	WTC		
	Autran_Epiphreatic3	558	WTC		
	Autran_Vadose1	182.4	VB		
	Autran_Vadose2	3404.2	VB		

Cave	Monogenic subdivision	Length (m)	Speleogenetic dominant process / Hydrodynamic zonation	Host rock formation	References
	Autran_Vadose3	971.9	VB		
Baume (Gr. De) (France, Herault)		602.8	AM	Upper jurassic (shaly limestone)	Bigot et al. (2015)
Baume Galiniere (Gr. De) (France, Vaucluse)		189	AM	Aptian (Urgonian limestone)	Audra et al. (2015b)
Brun (Eventde) (France, Gard)	Brun_Epiphreatic1	3454.5	LC	Middle Jurassic (Limestone and dolostone)	/
	Brun_Vadose2	177.2	VB		
	Brun_Vadose3	316.4	VB		
Carlsbad Cavern (USA, NM, Guadalu		66,316	AM	Permian (back-reef limestone)	Hill (1987); Polyak et al. (1998); Palmer and Palmer

Cave	Monogenic subdivision	Length (m)	Speleogenetic dominant process / Hydrodynamic zonation	Host rock formation	References
pe Mts.)					(2000); Polyak and Provencio (2001)
Cellagua (Spain, Cantabrie)		323.8	VB		/
Chamois (Gr. Des) (France, Alpes de haute Provence)	Chamois_Epiphreatic1	1702.9	LC	Upper cretaceous (limestone and shaly-limestone)	Nobécourt et al. (2008); Audra et al. (2015a)
	Chamois_Epiphreatic2	3599.8	LC		
	Chamois_Epiphreatic3	4471.4	LC		
	Chamois_River	1679.2	WTC		
	Chamois_Vadose1	222.9	VB		
	Chamois_Vadose2	291.3	VB		
Chapo (Spain, Cantabrie)		1080	VB	/	/

Cave	Monogenic subdivision	Length (m)	Speleogenetic dominant process / Hydrodynamic zonation	Host rock formation	References
Due Dong (Gr. de) (VietNam)		2355.7	WTC	/	/
Eau Relie (Aven) (France, Var)		677.5	VB	Upper cretaceous	Arfib (2016)
Foussoubie (Goulede) (France, Ardeche)		22,950.1	LC	Lower cretaceous (Urgonian limestone)	Mocochain et al. (2006); Jaillet et al. (2011); Sadier (2014)
Garma Ciega (Spain, Cantabrie)		7124.8	VB	/	/
Lali	Lali_Epiphreatic	3966.3	LC	/	/

Cave	Monogenic subdivision	Length (m)	Speleogenetic dominant process / Hydrodynamic zonation	Host rock formation	References
(Aven) (Apuan Alps, Italy)	Lali_Vadose	852.8	VB		
Lechuguilla (USA, NM, Guadalupe Mts.)		239,251.6	AM	Permian (back-reef limestone)	Palmer and Palmer (2000); Polyak and Provencio (2001); Palmer and Palmer (2012); Kirkland (2014)
Mazo Chico (Spain, Cantabrie)		12,008.6	VB	/	/
Nam Pakam (Gr. De) (VietNam)		9504.1	WTC	/	/

Cave	Monogenic subdivision	Length (m)	Speleogenetic dominant process / Hydrodynamic zonation	Host rock formation	References
Pigette 1 (Gr. De) (France, Alpes de haute Provence)		289.4	AM	Hauterivian (limestone and shaly limestone)	Audra et al., 2002, Audra et al., 2010
Pigette 2 (Gr. De) (France, Alpes de haute Provence)		456.3	AM		
Rubicera (Spain, Cantabrie)		4281.7	VB	/	/
Sakany (Gr. De) (France, Pyrenees)	Sakany_River	358.3	WTC	Lower cretaceous (Urgonian	Cassou and Bigot (2007)
	Sakany_MainCave	5831.5	LC		
	Sakany_Part2	456.5	LC		

Cave	Monogenic subdivision	Length (m)	Speleogenetic dominant process / Hydrodynamic zonation	Host rock formation	References
				limestone)	
Shuanghe Dongqun (China, Guizhou)	Shuanghe_Part1	24,215.4	WTC	Paleozoic carbonates	Song (1986); Zhang et al. (1992)
	Shuanghe_Part2	6429.2	WTC		
	Shuanghe_Part3	14,001.9	WTC		
	Shuanghe_Part4	53,398.1	WTC		
	Shuanghe_Vadose	1283.5	VB		
Saint-Benoit (Gr. de) (France, Alpes de Haute Provence)		2125.2	LC	Priabonian carbonates	Audra and Bigot, 2005, Audra and Bigot, 2009
Saint Marcel (Gr. De) (France,	StMarcel_LowerLevel	15,700.7	WTC	Lower cretaceous (Urgonia	Mocochain et al. (2006)
	StMarcel_MiddleLevel	19,422.4			

Cave	Monogenic subdivision	Length (m)	Speleogenetic dominant process / Hydrodynamic zonation	Host rock formation	References
Ardeche)	StMarcel_UpperLevel	12,430.1		n	
Saint Sebastien (Gr. de) (France, Alpes de haute Provence)		314	AM	Hauterivian (limestone and shaly limestone)	Audra and Bigot, 2005, Audra and Bigot, 2009
Total		621,037			

Appendix B. Values of morphometric parameters computed on the 56 cave samples (48 monogenic and 8 polygenic). Values for *WH* and *K* correspond to the mean of the computed values over the cave survey stations of a given cave sample, value for *T* correspond to the mean value computed over the cave branches. The others parameters are computed as one value per cave sample

Monogenetic type	**Cave samples names**	**Geometrical parameters**				**Topological parameters**					
		Vertical index (V)	**Width–height ratio (WH)**	**Curvature (K)**	**Tortuosity (T)**	**Node valence ratio (%)**			**Ramification index (R)**	**α**	**γ**
						ND_1	**ND_3**	**$ND_{>3}$**			
Vadose branchwork (VB)	Abisso Chimera	0.108	0.911	0.139	1.345	48.951	47.552	3.497	1.043	0.025	0.352
	Arrestelia_VadoseH	0.007	0.523	0.142	1.344	54.943	37.126	7.931	0.820	0.022	0.348
	Arrestelia_VadoseV	0.678	0.574	0.125	1.191	62.500	37.500	0.000	0.600	0.000	0.389
	Autran_Vadose1	0.610	0.650	0.281	1.613	100.000	0.000	0.000	0.000	0.000	1.000
	Autran_Vadose2	0.128	0.455	0.204	1.356	48.718	46.154	5.128	1.053	0.060	0.381
	Autran_Vadose3	0.311	0.143	0.235	1.488	75.000	25.000	0.000	0.333	0.000	0.500
	Brun_Vadose2	0.615	1.056	0.184	1.392	75.000	25.000	0.000	0.333	0.000	0.417

Monogenetic type	Cave samples names	Geometrical parameters				Topological parameters					
		Vertical index (V)	Width–height ratio (WH)	Curvature (K)	Tortuosity (T)	Node valence ratio (%)			Ramification index (R)	α	γ
						ND_1	ND_3	$ND_{>3}$			
	Brun_Vadose3	0.516	0.880	0.232	1.214	66.667	33.333	0.000	0.500	0.000	0.500
	Cellagua	0.744	0.249	0.167	1.339	100.000	0.000	0.000	0.000	0.000	1.000
	Chamois_Vadose1	0.363	0.298	0.187	1.277	75.000	25.000	0.000	0.333	0.000	0.500
	Chamois_Vadose2	0.563	0.673	0.180	1.147	66.667	33.333	0.000	0.500	0.000	0.417
	Chapo	0.230	0.429	0.115	1.276	56.000	40.000	4.000	0.786	0.000	0.348
	Eau Relie	0.192	0.170	0.387	1.251	47.368	47.368	5.263	1.111	0.034	0.378
	Garma Ciega	0.116	0.530	0.154	1.441	61.111	27.778	11.111	0.636	0.049	0.381
	Lali_Vadose	0.253	1.005	0.094	1.975	100.000	0.000	0.000	0.000	0.000	1.000
	Mazo Chico	0.060	0.542	0.245	1.259	52.381	42.857	4.762	0.909	0.034	0.358
	Rubicera	0.110	1.42	0.090	1.644	56.25	43.7	0.00	0.778	0.0	0.3

Monogenetic type	Cave samples names	Geometrical parameters				Topological parameters					
		Vertical index (V)	Width–height ratio (WH)	Curvature (K)	Tortuosity (T)	Node valence ratio (%)			Ramification index (R)	α	γ
						ND_1	ND_3	$ND_{>3}$			
			6			0	50	0		00	57
	Shuanghe_Vadose	0.286	0.574	0.098	1.288	62.500	37.500	0.000	0.600	0.000	0.389
Water-table cave (WTC)	Autran_Epiphreatic1	0.038	1.550	0.168	1.394	60.000	40.000	0.000	0.667	0.000	0.375
	Autran_Epiphreatic2	0.044	2.421	0.204	1.242	61.538	30.769	7.692	0.625	0.080	0.410
	Autran_Epiphreatic3	0.029	1.200	0.160	1.170	57.143	42.857	0.000	0.750	0.000	0.361
	Chamois_River	0.030	2.581	0.066	1.287	53.846	38.462	7.692	0.857	0.048	0.394
	Due Dong	0.035	1.400	0.029	1.354	58.333	41.667	0.000	0.714	0.000	0.367
	Nam Pakan	0.013	1.819	0.096	1.131	51.087	44.565	4.348	0.957	0.016	0.348
	Sakany_Sakany_River	0.021	3.118	0.136	1.178	61.538	30.769	7.692	0.625	0.000	0.364
	Shuanghe_Part1	0.015	1.521	0.061	1.175	53.125	43.229	3.646	0.882	0.008	0.333

Monogenetic type	Cave samples names	Geometrical parameters				Topological parameters					
		Vertical index (V)	Width–height ratio (WH)	Curvature (K)	Tortuosity (T)	Node valence ratio (%)			Ramification index (R)	α	γ
						ND_1	ND_3	$ND_{>3}$			
	Shuanghe_Part2	0.024	1.521	0.065	1.290	47.222	52.778	0.000	1.118	0.030	0.363
	Shuanghe_Part3	0.013	1.521	0.062	1.227	47.475	49.495	3.030	1.106	0.026	0.354
	Shuanghe_Part4	0.006	1.521	0.070	1.222	49.024	46.829	4.146	1.040	0.023	0.346
	StMarcel_Lower Level	0.006	1.720	0.141	1.285	45.714	51.429	2.857	1.188	0.042	0.364
	StMarcel_Middle Level	0.005	2.509	0.116	1.217	45.933	49.761	4.306	1.177	0.038	0.359
	StMarcel_Upper Level	0.006	2.355	0.176	1.191	48.790	45.161	6.048	1.050	0.031	0.354
Looping cave (LC)	Brun_Epiphreatic1	0.024	1.459	0.102	1.315	52.941	41.176	5.882	0.889	0.015	0.353
	Chamois_Epiphreatic1	0.028	1.908	0.215	1.138	37.647	51.765	10.588	1.656	0.102	0.405
	Chamois_Epiphreatic2	0.029	1.854	0.136	1.130	47.059	47.899	5.042	1.125	0.034	0.359
	Chamois_Epiphr	0.030	1.81	0.096	1.080	50.00	41.8	8.14	1.000	0.0	0.3

Monogenetic type	Cave samples names	Geometrical parameters				Topological parameters					
		Vertical index (V)	Width–height ratio (WH)	Curvature (K)	Tortuosity (T)	Node valence ratio (%)			Ramification index (R)	α	γ
						ND_1	ND_3	$ND_{>3}$			
	eatic3		5			0	60	0		34	56
	Foussoubie	0.006	1.317	0.130	1.232	39.474	58.187	2.339	1.533	0.061	0.375
	Lali_Epiphreatic	0.033	1.650	0.108	1.150	49.333	46.667	4.000	1.027	0.021	0.352
	Sakany_MainCave	0.024	0.706	0.345	1.445	50.824	42.857	6.319	0.968	0.024	0.345
	Sakany_Part2	0.172	1.058	0.323	1.227	52.778	41.667	5.556	0.895	0.015	0.353
	St Benoit	0.036	2.763	0.218	1.168	49.020	49.020	1.961	1.040	0.015	0.346
Angular maze (AM)	Baume	0.057	1.897	0.345	1.177	49.398	38.554	12.048	1.024	0.073	0.393
	Baume Galiniere	0.057	1.059	0.326	1.106	56.667	26.667	16.667	0.765	0.048	0.369
	Carlsbad Cavern	0.005	1.632	0.235	1.164	37.020	47.080	15.900	1.701	0.113	0.409
	Lechuguilla	0.006	2.119	0.231	1.214	39.483	44.971	15.546	1.551	0.110	0.406

Monogenetic type	Cave samples names	Geometrical parameters				Topological parameters					
		Vertical index (V)	Width–height ratio (WH)	Curvature (K)	Tortuosity (T)	Node valence ratio (%)			Ramification index (R)	α	γ
						ND_1	ND_3	$ND_{>3}$			
	Pigette 1	0.121	1.731	0.475	1.262	51.724	37.931	10.345	0.933	0.038	0.370
	Pigette 2	0.111	1.613	0.386	1.235	44.231	55.769	0.000	1.261	0.040	0.367
	Saint Sebastien	0.027	1.625	0.273	1.049	52.174	34.783	13.043	0.917	0.034	0.364
Polygenic network (PN)	Arrestelia	0.013	0.516	0.143	1.343	54.909	37.215	7.877	0.821	0.022	0.348
	Autran	0.062	0.706	0.211	1.279	49.711	46.821	3.468	1.012	0.040	0.362
	Brun	0.042	1.509	0.118	1.305	50.847	44.068	5.085	0.967	0.017	0.350
	Chamois	0.026	1.830	0.140	1.123	44.277	47.892	7.831	1.259	0.052	0.369
	Lali	0.059	1.501	0.105	1.154	49.351	46.753	3.896	1.026	0.020	0.351
	Sakany	0.022	0.807	0.338	1.420	49.878	43.309	6.813	1.005	0.024	0.347
	Shuanghe	0.005	1.33	0.069	1.215	49.20	47.0	3.73	1.033	0.0	0.3

Monogenetic type	Cave samples names	Geometrical parameters				Topological parameters					
		Vertical index (V)	Width–height ratio (WH)	Curvature (K)	Tortuosity (T)	Node valence ratio (%)			Ramification index (R)	α	γ
						ND_1	ND_3	$ND_{>3}$			
			1			0	67	3		19	44
	Saint Marcel	0.005	2.201	0.118	1.230	45.923	48.918	5.158	1.178	0.039	0.360

Appendix C. Relationships between α and γ

In the case of planar graphs, it α and γ are defined as follows:

$$\alpha = E - N + 12N - 5$$

and

$$\gamma = E3N - 2.$$

It is possible to define E (number of edges) as a function of γ as follows:

$$E = 3N - 2\gamma$$

Then, E can be inserted in the equation of α, yielding:

$$\alpha = 3N - 2\gamma - N + 12N - 5 = 3N - 22N - 5\gamma - N - 12N - 5$$

If N tends to $+\infty$, then the asymptotes of the two fractions are:

$$\lim N \to +\infty 3N - 22N - 5 = 32$$

$$\lim N \to +\infty N - 12N - 5 = 12$$

If N is huge, a linear relationships may exist between α and γ which can be written as follows

$$\alpha \approx 32\gamma - 12$$

Or

$$\gamma \approx 23\alpha + 13$$

References

Albert et al., 2015
G. Albert, M. Virag, A. Eross**Karst porosity estimations from archive cave surveys - studies in the Buda Thermal Karst System (Hungary)**
Int. J. Speleol., 44 (2) (2015), pp. 151-165, 10.5038/1827-806X.44.2.5
Arfib, 2016
B. Arfib**La géologie du gouffre de l'Eau-Relie en Provence**
(2016), pp. 1-18
(hal-01450992)
http://www.karsteau/telechargement/GeologieEauRelie_BrunoArfib.pdf
Audra, 2007
P. Audra**Karst et spéléogenèses épigènes, hypogènes, recherches appliquées et valorisation**
University of Nice Sophia-Antipolis, Hab. thesis (2007)
(278 pp)
Audra and Bigot, 2005
P. Audra, J.Y. Bigot**La grotte de Saint-Benoit: un modèle de cavité épinoyée. Méailles et la région d'Annot. Paysages culturels karstiques. Architecture d'une relation homme-territoire unique**

Université de Nice Sophia Antipolis, département de Géographie (2005)
Audra and Bigot, 2009
P. Audra, J.Y. Bigot**Les grottes de Saint Benoit**
Spelunca, 114 (2009)
Audra and Palmer, 2013
P. Audra, A.N. Palmer**The vertical dimension of karst: controls of vertical cave pattern**
J.E.I.C. Shroder, A.E. Frumkin (Eds.), Treatise on Geomorphology, Academic Press, Karst Geomorphology (2013), pp. 186-206
Audra and Palmer, 2015
P. Audra, A.N. Palmer**Research frontiers in speleogenesis. Dominant processes, hydrogeological conditions and resulting cave patterns**
Acta Carsologica, 44 (3) (2015), 10.3986/ac.v44i3.1960
Audra et al., 2002
P. Audra, J.Y. Bigot, L. Mocochain**Hypogenic caves in Provence (France). Specific features and sediments**
Acta Carsologica, 31 (3) (2002), pp. 33-50, 10.3986/ac.v31i3.378
View Record in Scopus
Audra et al., 2010
P. Audra, J.C. D'Antoni-Nobecourt, J.Y. Bigot**Hypogenic caves in France. Speleogenesis and morphology of the cave systems**
B Soc Geol Fr, 181 (4) (2010), pp. 327-335, 10.2113/gssgfbull.181.4.327
Audra et al., 2015a
P. Audra, F. Gazquez, F. Rull, J.Y. Bigot, H. Camus**Hypogene Sulfuric Acid Speleogenesis and rare sulfate minerals in Baume Galiniere Cave (Alpes-de-Haute-Provence, France). Record of uplift, correlative cover retreat and valley dissection**
Geomorphology, 247 (2015), pp. 25-34, 10.1016/j.geomorph.2015.03.031
Audra et al., 2015b
P. Audra, J.C. Nobécourt, J.Y. Bigot**Sixième camp international d'exploration « Chamois 2014 »**
Spelunca (2015), pp. 31-40
Barthélemy, 2011
M. Barthélemy**Spatial networks**
Phys. Rep., 499 (1–3) (2011), pp. 1-101, 10.1016/j.physrep.2010.11.002
Bigot et al., 2015
J.Y. Bigot, H. Camus, P. Audra**Une nouvelle grotte hypogène en Languedoc: La grotte de la Baume**
Cardabelle (CLPA). (2015)

Bonacci et al., 2006
O. Bonacci, I. Ljubenkov, T. Roje-Bonacci**Karst flash floods: an example from the Dinaric karst (Croatia)**
Nat Hazard Earth Sys, 6 (2) (2006), pp. 195-203
Borghi et al., 2012
A. Borghi, P. Renard, S. Jenni**A pseudo-genetic stochastic model to generate karstic networks**
J. Hydrol., 414 (2012), pp. 516-529, 10.1016/j.jhydrol.2011.11.032
Borghi et al., 2016
A. Borghi, P. Renard, F. Cornaton**Can one identify karst conduit networks geometry and properties from hydraulic and tracer test data?**
Adv. Water Resour., 90 (2016), pp. 99-115, 10.1016/j.advwatres.2016.02.009
Brice, 1960
J.C. Brice**Index for description of channel braiding**
Geol. Soc. Am. Bull., 71 (1960), p. 1833
Bruthans et al., 2010
J. Bruthans, M. Filippi, M. Zare, Z. Churáčková, N. Asadi, M. Fuchs, J. Adamovi č**Evolution of salt diapir and karst morphology during the last glacial cycle: Effects of sea-level oscillation, diapir and regional uplift, and erosion (Persian Gulf, Iran)**
Geomorphology, 121 (3–4) (2010), pp. 291-304, 10.1016/j.geomorph.2010.04.026
Cassou and Bigot, 2007
J.P. Cassou, J.Y. Bigot**Le labyrinthe de la grotte de Sakany (Quié, Ariège)**
Actes de la 17e Rencontre d'Octobre, 29-36 (2007)
Cochran, 1977
W.G. Cochran**Sampling Techniques**
(3rd Edition), Wiley (1977)
Collon et al., 2017
P. Collon, D. Bernasconi, C. Vuilleumier, P. Renard**Statistical metrics for the characterization of karst network geometry and topology**
Geomorphology, 283 (2017), pp. 122-142, 10.1016/j.geomorph.2017.01.034
Collon-Drouaillet et al., 2012
P. Collon-Drouaillet, V. Henrion, J. Pellerin**An algorithm for 3D simulation of branchwork karst networks using Horton parameters and A* Application to a synthetic case**
Geol. Soc. Lond., Spec. Publ., 370 (1) (2012), pp. 295-306, 10.1144/SP370.3

Columbu et al., 2015
A. Columbu, J. De Waele, P. Forti, P. Montagna, V. Picotti, E. Pons-Branchu, J. Hellstrom, P. Bajo, R. Drysdale**Gypsum caves as indicators of climate-driven river incision and aggradation in a rapidly uplifting region**
Geology, 43 (6) (2015), pp. 539-542, 10.1130/g36595.1
De Waele et al., 2016
J. De Waele, P. Audra, G. Madonia, M. Vattano, L. Plan, I.M. D'Angeli, J.-Y. Bigot, J.-C.Nobécourt**Sulfuric acid speleogenesis (SAS) close to the water table: examples from southern France, Austria, and Sicily**
Geomorphology, 253 (2016), pp. 452-467, 10.1016/j.geomorph.2015.10.019
Egozi and Ashmore, 2008
R. Egozi, P. Ashmore**Defining and measuring braiding intensity**
Earth Surf. Process. Landf., 33 (2008), pp. 2121-2138, 10.1002/esp.1658
Filipponi et al., 2009
M. Filipponi, P.Y. Jeannin, L. Tacher**Evidence of inception horizons in karst conduit networks**
Geomorphology, 106 (1–2) (2009), pp. 86-99, 10.1016/j.geomorph.2008.09.010
Filipponi et al., 2010
M. Filipponi, P.Y. Jeannin, L. Tacher**Understanding cave genesis along favourable bedding planes. The role of the primary rock permeability**
Z. Geomorphol., 54 (2) (2010), pp. 91-114, 10.1127/0372-8854/2010/0054S2-0006
Ford, 1971
D.C. Ford**Geologic structure and a new explanation of limestone cavern genesis**
Transactions of the Cave Research Group of Great Britain., 13 (2) (1971), pp. 81-94
Ford and Williams, 1989
D.C. Ford, P.W. Williams**Karst Geomorphology and Hydrology, London** (1989)
Ford and Williams, 2007
D.C. Ford, P.W. Williams**Karst Hydrogeology and Geomorphology, Chichester**
(2007)
Fournillon et al., 2012

A. Fournillon, S. Abelard, S. Viseur, B. Arfib, J. Borgomano**Characterization of karstic networks by automatic extraction of geometrical and topological parameters: comparison between observations and stochastic simulations**
Geol. Soc. Spec. Publ., 370 (2012), pp. 247-264, 10.1144/SP370.8
Frumkin and Fischhendler, 2005
A. Frumkin, I. Fischhendler**Morphometry and distribution of isolated caves as a guide for phreatic and confined paleohydrological conditions**
Geomorphology, 67 (3–4) (2005), pp. 457-471, 10.1016/j.geomorph.2004.11.009
Gabrovšek et al., 2014
F. Gabrovšek, P. Häuselmann, P. Audra**‘Looping caves’ versus ‘water table caves’: the role of base-level changes and recharge variations in cave development**
Geomorphology, 204 (2014), pp. 683-691, 10.1016/j.geomorph.2013.09.016
Garrison, 1960
W.L. Garrison**Connectivity of the interstate highway system**
Pap. Reg. Sci., 6 (1) (1960), pp. 121-137
Goldscheider et al., 2008
N. Goldscheider, J. Meiman, M. Pronk, C. Smart**Tracer tests in karst hydrogeology and speleology**
Int. J. Speleol., 37 (1) (2008), pp. 27-40
https://doi.org/10.5038/1827-806X.37.1.3
Haggett and Chorley, 1969
P. Haggett, R.J. Chorley**Network Analysis in Geography**
Edward Arnold, London (1969)
Harmand et al., 2017
D. Harmand, K. Adamson, G. Rixhon, S. Jaillet, B. Losson, A. Devos, G. Hez, M . Calvet, P.Audra**Relationships between fluvial evolution and karstification related to climatic, tectonic and eustatic forcing in temperate regions**
Quat. Sci. Rev. (2017), 10.1016/j.quascirev.2017.02.016
Hartmann et al., 2014
A. Hartmann, N. Goldscheider, T. Wagener, J. Lange, M. Weiler**Karst water resources in a changing world: review of hydrological modeling approaches**
Rev. Geophys., 52 (3) (2014), pp. 218-242, 10.1002/2013RG000443
Häuselmann, 2002

P. Häuselmann**Cave Genesis and Its Relation to Surface Processes: Investigation in the Siebenhengste Region (BE, Switzerland)**
PhD thesis
University of Fribourg, Switzerland (2002)
(168 pp)
Häuselmann et al., 2003
P. Häuselmann, P.Y. Jeannin, M. Monbaron**Role of epiphreatic flow and soutirages in conduit morphogenesis: the Bärenschacht Example (BE, Switzerland)**
Z. Geomorphol., 47 (2) (2003), pp. 171-190
Hendrick and Renard, 2016
M. Hendrick, P. Renard**Fractal dimension, walk dimension and conductivity exponent of Karst networks around Tulum**
Frontiers in Physics, 4 (2016), 10.3389/fphy.2016.00027
Henrion, 2011
V. Henrion**Approche pseudo-génétique pour la simulation stochastique de la géométrie 3D de réseaux de fractures et karstiques**
PhD thesis
Institut National Polytechnique de Lorraine (2011)
(155 pp)
Hill, 1987
C.A. Hill**Geology of Carlsbad cavern and other caves in the Guadalupe Mountains, New Mexico and Texas**
New Mexico Bureau of Mines and Mineral Resources, 117 (1987), pp. 1-150
Hollander et al., 2013
M. Hollander, D.A. Wolfe, E. Chicken**Nonparametric Statistical Methods** (3rd Edition), John Wiley & Sons (2013)
Hong and Davies, 1979
L.B. Hong, T.R.H. Davies**A study of stream braiding**
Geol. Soc. Am. Bull., 90 (2) (1979), pp. 1839-1859
Howard, 1971
A.D. Howard**Quantitative measures of cave patterns. Caves and karst**
Research in speleology, 13 (1) (1971), pp. 1-7
Howard et al., 1970
A.D. Howard, M.E. Keetch, C.L. Vincent**Topological and geometrical properties of braided streams**
Water Resour. Res., 6 (6) (1970), pp. 1674-1688, 10.1029/WR006i006p01674
Huntoon, 1995

P.W. Huntoon**Is it appropriate to apply porous media groundwater circulation models to karstic aquifers?**
A.I. El-Kadi (Ed.), Assesment of Model for Groundwater Resource Analysis and Management, Lewis Publishers, Boca Raton, Florida (1995), pp. 339-358
Jacek, 2015
S. Jacek**Cave development in an uplifting fold-and-thrust belt: case study of the Tatra Mountains, Poland**
Int. J. Speleol., 44 (3) (2015), pp. 341-359, 10.5038/1827-806X.44.3.10
Jaillet et al., 2011
S. Jaillet, B. Sadier, J. Arnaud, M. Azma, E. Boche, D. Cailhol, M. Filipponi, P. R oux, E. Varrel**Topographie, représentation et analyse morphologique 3D de drains, de conduits et de parois du karst. Images et modèles 3D en milieux naturels, edytem edition., 12. CNRS**
(2011)
Jaquet et al., 2004
O. Jaquet, P. Siegel, G. Klubertanz, H. Benabderrhamane**Stochastic discrete model of karstic networks**
Adv. Water Resour., 27 (7) (2004), pp. 751-760, 10.1016/j.advwaters.2004.03.007
Jeannin, 1996
P.Y. Jeannin**Structure et comportement hydraulique des aquifères karstiques**
(1996)
PhD Dissertation. (237 pp)
Jeannin et al., 2007
P.Y. Jeannin, C. Groves, P. Häuselmann**Speleological investigations**
N. Goldscheider, D. Drew (Eds.), Methods in Karst Hydrogeology, Taylor & Francis, London (2007), pp. 25-44
Kirkland, 2014
D.W. Kirkland**Role of hydrogen sulfide in the formation of cave and karst phenomena in the Guadalupe Mountains and western Delaware Basin, New Mexico and Texas**
Special Paper Series 1 (2014)
Klimchouk, 2007
A. Klimchouk**Hypogene speleogenesis: hydrogeological and morphogenetic perspective**
Special Paper no.1 (2007)
Klimchouk, 2009
A. Klimchouk**Morphogenesis of hypogenic caves**

Geomorphology, 106 (1–2) (2009), pp. 100-117, 10.1016/j.geomorph.2008.09.013
Klimchouk and Ford, 2000
A. Klimchouk, D.C. Ford**Lithological and structural controls of dissolutional cave development**
A. Klimchouk, D.C. Ford, A.N. Palmer, W. Dreybrodt (Eds.), Speleogenesis: Evolution of Karst Aquifers, National Speleological Society (2000), p. 527
Klimchouk et al., 2016
A. Klimchouk, A.S. Auler, F.H.R. Bezerra, C.L. Cazarin, F. Balsamo, Y. Dublyan sky**Hypogenic origin, geologic controls and functional organization of a giant cave system in Precambrian carbonates, Brazil**
Geomorphology, 253 (2016), pp. 385-405, 10.1016/j.geomorph.2015.11.002
Littva et al., 2015
J. Littva, J. Hok, P. Bella**Cavitonics: Using caves in active tectonic studies (Western Carpathians, case study)**
J. Struct. Geol., 80 (2015), pp. 47-56, 10.1016/j.jsg.2015.08.011
Martel, 1921
E.A. Martel**Nouveau traité des eaux souterraines**
Doin, Paris (1921)
Mocochain et al., 2006
L. Mocochain, G. Clauzon, J.Y. Bigot, P. Brunet**Geodynamic evolution of the peri-Mediterranean karst during the Messinian and the Pliocene: evidence from the Ardeche and Rhone Valley systems canyons, Southern France**
Sediment. Geol., 188 (2006), pp. 219-233, 10.1016/j.sedgeo.2006.03.006
Mosley, 1981
P. Mosley**Semi-determinate hydraulic geometry of river channels, South Island, New Zealand**
Earth Surf. Process. Landf., 6 (2) (1981), pp. 127-137, 10.1002/esp.3290060206
Nobécourt et al., 2008
J.C. Nobécourt, P. Audra, J.Y. Bigot**Le karst du Grand Coyer. Explorations à la source du Coulomp (Alpes-de-Hautes-Provence)**
Actes de la 18e Rencontre d'Octobre (2008)
Palmer, 1972
A.N. Palmer**Dynamics of a sinking stream system: Onesquetaw Cave**
National Speleological Society Bulletin, 34 (3) (1972), pp. 89-110
Palmer, 1975
A.N. Palmer**The origin of maze caves**

The NSS Bulletin, 37 (3) (1975), pp. 56-76
Palmer, 1991
A.N. Palmer**Origin and morphology of limestone caves**
Geol. Soc. Am. Bull., 103 (1) (1991), pp. 1-21, 10.1130/0016-7606(1991)103<0001:Oamolc>2.3.Co;2
Palmer, 2007
A.N. Palmer**Cave Geology**
Cave books, Dayton, OH (2007)
Palmer and Palmer, 2000
A.N. Palmer, M.V. Palmer**Hydrochemical interpretation of cave patterns in the Guadalupe Mountains, New Mexico**
Journal of Cave and Karst Studies, 62 (2) (2000), pp. 91-108
Palmer and Palmer, 2012
M.V. Palmer, A.N. Palmer**Petrographic and isotopic evidence for late-stage processes in sulfuric acid caves of the Guadalupe Mountains, New Mexico, USA**
Int. J. Speleol., 41 (2) (2012), pp. 231-250, 10.5038/1827-806X.41.2.10
Pardo-Igúzquiza et al., 2011
E. Pardo-Igúzquiza, J.J. Duran-Valsero, V. Rodriguez-Galiano**Morphometric analysis of three-dimensional networks of karst conduits**
Geomorphology, 132 (1–2) (2011), pp. 17-28, 10.1016/j.geomorph.2011.04.030
Pardo-Igúzquiza et al., 2012
E. Pardo-Igúzquiza, P.A. Dowd, C. Xu, J.J. Durán-Valsero**Stochastic simulation of karst conduit networks**
Adv. Water Resour., 35 (2012), pp. 141-150, 10.1016/j.advwatres.2011.09.014
Peterson and Wicks, 2006
E.W. Peterson, C.M. Wicks**Assessing the importance of conduit geometry and physical parameters in karst systems using the storm water management model (SWMM)**
J. Hydrol., 329 (1–2) (2006), pp. 294-305, 10.1016/j.jhydrol.2006.02.017
Piccini, 2011
L. Piccini**Recent developments on morphometric analysis of karst caves**
Acta Carsologica, 40 (1) (2011), pp. 43-52
https://doi.org/10.3986/ac.v40i1.27
Ployon et al., 2011

E. Ployon, S. Jaillet, O. Barge**Acquisition et traitements de nuages de points 3D par des techniques légères et à faible coûts pour l'élaboration de MNT à haute résolution**
S. Jaillet, E. Ployon, T. Villemin (Eds.), Images et modèles 3D en milieux naturels, Edytem edition, CNRS(2011), pp. 155-168
Polyak and Provencio, 2001
V.J. Polyak, P. Provencio**By-product materials related to H2S–H2SO4-influenced speleogenesis of Carlsbad, Lechuguilla, and other caves of the Guadalupe Mountains, New Mexico**
Journal of Cave and Karst Studies, 63 (1) (2001), pp. 23-32
Polyak et al., 1998
V.J. Polyak, W.C. McIntosh, P. Provencio, N. Güven**Age and origin of Carlsbad Caverns and related caves from 40Ar/39Ar of alunite**
Science, 279 (1998), pp. 1919-1922, 10.1126/science.279.5358.1919
Renard, 2007
P. Renard**Stochastic hydrogeology: what professionals really need?**
Ground Water, 45 (5) (2007), pp. 531-541, 10.1111/j.1745-6584.2007.00340.x
Renard, 2014
P. Renard**How to Quantify the Quality of Karst Network Models?**
American Geophysical Union, Fall Meeting (2014), p. 06
Renault, 1970
P. Renault**La formation des cavernes. coll. “Que sais-je ?”, 1400**
Armand Colin, Paris (1970)
Rodrigue et al., 2006
J.P. Rodrigue, C. Comtois, B. Slack**The geography of transport systems**
N. Y. (2006)
Rongier et al., 2014
G. Rongier, P. Collon, M. Filipponi**Simulation of 3D karst conduits with an object-distance based method integrating geological knowledge**
Geomorphology, 217 (2014), pp. 152-164, 10.1016/j.geomorph.2014.04.024
Sadier, 2014
B. Sadier**3D et géomorphologie karstique : La grotte Chauvet et les cavités des Gorges de l'Ardèche**
PhD Dissertation
Université de Grenoble (2014)
Saporta, 2006
G. Saporta**Probabilités**
(2006)

(Analyse des données et statistique)
Sauro, 2014
F. Sauro**Structural and lithological guidance on speleogenesis in quartz-sandstone: evidence of the arenisation process**
Geomorphology, 226 (2014), pp. 106-123, 10.1016/j.geomorph.2014.07.033
Song, 1986
L. Song**Karst geomorphology and subterranean drainage in south Dushan**
Guizhou Province, China. Cave Science, 13 (2) (1986), pp. 49-63
Taaffe and Gauthier, 1973
E.J. Taaffe, H.L. Gauthier**Geography of Transportation**
Prenctice Hall, Englewood Cliffs, New Jersey (1973)
Tîrlă and Vijulie, 2013
L. Tîrlă, I. Vijulie**Structural–tectonic controls and geomorphology of the karst corridors in alpine limestone ridges: Southern Carpathians, Romania**
Geomorphology, 197 (2013), pp. 123-136, 10.1016/j.geomorph.2013.05.003
Viseur et al., 2014
S. Viseur, J. Jouves, A. Fournillon, B. Arfib**3D stochastic simulation of caves: application to St-Sebastien case study (SE, France)**
Karstologia, 64 (2014), pp. 17-24
Worthington, 1999
S.R.H. Worthington**A comprehensive strategy for understanding flow in carbonate aquifers**
A.N. Palmer, M.V. Palmer, I.D. Sasowsky (Eds.), Karst Modelling, Karst Waters Institute, Charlottesville, Virginia (1999), pp. 30-37
Worthington and Ford, 2009
S.R.H. Worthington, D.C. Ford**Self-organized permeability in carbonate aquifers**
Ground Water, 47 (3) (2009), pp. 326-336, 10.1111/j.1745-6584.2009.00551.x
Zhang et al., 1992
Y. Zhang, M. Yang, C. He**Karst geomorphology and environmental implications in Guizhou, China**
Cave Science, 19 (1992), pp. 13-20